

Galactosynthesis: Halo Histories, Star Formation, and Disks

Ari Buchalter¹, Raul Jimenez² & Marc Kamionkowski¹

¹Theoretical Astrophysics Group, Mail Code 130-33, California Institute of Technology, Pasadena, CA 91125.

ari@tapir.caltech.edu, kamion@tapir.caltech.edu

²Institute for Astronomy, University of Edinburgh, Blackford Hill, Edinburgh EH9 3HJ, UK.

raul@roe.ac.uk

27 October 2018

ABSTRACT

We investigate the effects of a variety of ingredients that must enter into a realistic model for disk-galaxy formation, focusing primarily on the Tully-Fisher (TF) relation and its scatter in several wavebands. In particular, we employ analytic distributions for halo-formation redshifts and halo spins, empirical star-formation rates and initial mass functions, realistic stellar populations, and chemical evolution of the gas. Our main findings are: (a) the slope, normalization, and scatter of the TF relation across various wavebands is determined *both* by halo properties and star formation in the disk; (b) TF scatter owes primarily to the spread in formation redshifts. The scatter can be measurably reduced by chemical evolution, and also in some cases by the weak anti-correlation between peak height and spin; (c) multi-wavelength constraints can be important in distinguishing between models which appear to fit the TF relation in *I* or *K*; (d) successful models seem to require that the bulk of disk formation cannot occur too early ($z > 2$) or too late ($z < 0.5$), and are inconsistent with high values of Ω_0 ; (e) a realistic model with the above ingredients can reasonably reproduce the observed $z = 0$ TF relation in *all* bands (*B*, *R*, *I*, and *K*). It can also account for the $z = 1$ *B*-band TF relation and yield rough agreement with the local *B* and *K* luminosity functions and *B*-band surface-brightness–magnitude relation. In such a model, the near-infrared TF relation at $z = 1$ is similar to that at $z = 0$, while bluer bands show a markedly steeper TF slope at high redshift. The remarkable agreement with observations suggests that the amount of gas that is expelled or poured into a disk galaxy must be small (though small fluctuations might serve to better align *B*-band predictions with observations), and that the specific angular momentum of the baryons must roughly equal that of the halo; there is little room for angular momentum transfer. In an appendix we present analytic fits to stellar-population synthesis models.

Key words: cosmology: theory—galaxies: formation—galaxies: spiral—galaxies: kinematics and dynamics.

1 INTRODUCTION

Spiral galaxies are particularly important in the study of galaxy formation, as they are believed to undergo a relatively smooth formation process, and serve as the building blocks in the formation of other galactic systems through mergers. Thus, spiral galaxies should be the easiest to model and should provide clues as to the basic physics underlying galaxy formation. Various lines of observational evidence serve to guide our understanding of spirals, including their measured luminosity function (LF), surface-brightness distribution, star-formation history, chemical composition, and dynamical properties. Of particular significance is the Tully-Fisher (TF) relation, a remarkably tight correlation between the luminosity and rotation speed of spirals. For a given wavelength, λ , the TF relation obeys the form $L_\lambda = A_\lambda V_c^{\gamma_\lambda}$, or

$$M_\lambda = a_\lambda + b_\lambda \log V_c, \quad (1)$$

where M_λ is the absolute magnitude^{*}, and $b_\lambda = -2.5\gamma_\lambda$ is the slope of the relation. The debate continues as to whether this relationship results primarily from initial conditions, i.e., from the properties of the parent halo (Dalcanton, Spergel, & Summers 1997; Mo, Mao, & White 1998; Firmani & Avila-Reese 1998; Avila-Reese, Firmani, & Hernandez 1998; Navarro & Steinmetz 2000; Mo & Mao 2000), self-regulating feedback processes associated with star formation in the disk (Silk 1997), or a combination of both (Heavens & Jimenez 1999; Somerville & Primack 1999; van den Bosch 2000).

A TF relation arises quite naturally if one simply assumes that galactic halos formed at roughly the same time and that luminosity

^{*} A subscripted M is understood to refer to absolute magnitude in a given band, while an M without a subscript refers to mass.

is proportional to the baryonic mass, which is in turn proportional to the halo mass. More realistically, the luminosity may depend on the galactic spin, as disks formed in high-spin halos will be larger and thinner, and thus lead to lower star-formation rates. Still, even with spin, a TF relation arises if halos all formed at roughly the same epoch. In both cases (with and without spin), scatter in the redshift of halo formation should lead to scatter in the central densities of the halos and thus to scatter in the TF relation.

Several groups have made considerable progress in understanding spiral-galaxy properties along these lines using semi-analytical models (SAMs). Eisenstein & Loeb (1996, hereafter EL96) used Monte-Carlo realizations of halo-formation histories to calculate the minimum TF scatter which should arise from the spread in halo-formation times. They concluded that unless spirals form at $z \gtrsim 1$, without subsequently accreting much mass, the TF relation cannot arise simply from initial conditions, but must instead owe to some feedback mechanism which decouples the luminosity from the halo history.

More recently, other groups have investigated detailed SAMs of disk-galaxy formation which incorporate such features as formation histories derived directly from N -body simulations, universal halo profiles, adiabatic disk contraction, bulge formation via stability criteria, star formation, supernova feedback, dust, cooling, and mergers (Somerville & Primack 1999; van den Bosch 2000; Firmani & Avila-Reese 1998; Navarro & Steinmetz 2000). Their conclusions differ as to the relative importance of initial conditions vs. feedback from star formation and/or supernovae in defining the TF relation. These studies generally agree, however, that the spread in halo-formation redshifts is a significant source of scatter in the TF relation and that reconciling models with TF observations seems to require a low matter density ($\Omega_0 \sim 0.3 - 0.5$) and disk formation at high redshift ($z \gtrsim 1$).

One powerful test of such models, which has not been fully appreciated, is the simultaneous comparison of their predictions to TF data from *several* wavebands. Some previous work has considered only an assumed value for the mass-to-light ratio in a given band, rather than using stellar population models to predict broad-band magnitudes, and many authors have investigated TF predictions for only a single waveband, typically I or K , where the observed TF scatter is the smallest [~ 0.4 mag in the most carefully defined samples (Willick *et al.* 1995, 1996, 1997; Tully *et al.* 1998)]. Since these wavelengths measure primarily the oldest, shell-burning, stellar populations, such measurements are, by construction, effectively probing only the total mass of the galaxy. Thus, while some authors have claimed success in fitting the near-IR TF relation, their predictions in bluer bands, where many model ingredients would be most strongly manifested owing to the younger populations probed, have gone unchecked. With realistic stellar-population models, the leverage gained by spanning a range of wavelengths should therefore be crucial in distinguishing models which produce similar near-infrared TF predictions, and help to assess the importance of various SAM features. Heavens and Jimenez (1999; hereafter HJ99), used a simple halo and disk model combined with empirical star-formation properties to investigate the role of star formation in the TF relation, did examine the simultaneous constraints from various wavebands, but did not address some of the other key considerations listed above.

Our approach here will focus on constructing, as much as possible, a model “from the ground up,” i.e., starting with a minimal set of simple, well-motivated assumptions, and individually investigating the impact of various plausible modifications. In essence, we are asking whether a plausible model with fewer free param-

eters[†] than are usually incorporated into current SAMs can reasonably pass various observational tests. Though the resulting model will lack many of the sophisticated features of other SAMs and will surely be an oversimplification in many respects, it may shed important light on the issue of which physical ingredients are truly essential in determining certain disk properties.

We build on the work of HJ99, using their halo/disk model and stellar populations code, but generalizing it to include a variety of important features, such as analytic models for the distribution of halo-formation redshifts and spins (as well as the predicted anti-correlation between the two). This allows us to assess not only the impact of these distributions on TF predictions, but the dependence on cosmological parameters and the power spectrum as well. We also include for the first time an analytic description of chemical evolution. This measurably reduces the scatter in the TF relation, which is found to arise mainly from the spread in formation times. The overall result will be a model for disk galaxies which passes a host of observational tests, reproducing the observed TF relation, locally and at $z = 1$, in all relevant wavebands *with the right magnitude of scatter*. It also succeeds in roughly fitting the observed surface-brightness distribution of spirals and, within its limitations, reasonably reproduces the observed B - and K -band luminosity functions. The model necessitates cosmological parameter values which are in line with current estimates, and requires that the bulk of disk formation occur in the range $0.5 < z < 2$. This agreement implies that, although plausible, other mechanisms which would add or remove gas from the disk (such as mergers, gas expulsion by supernovae, etc.), and thereby distort the predicted luminosity, are not necessarily required to successfully predict these global disk-galaxy properties.

2 THE MODEL

2.1 Our Starting Point

We build on the skeletal disk-galaxy model of HJ99. We review the basic ingredients here and refer the reader to HJ99 for a more complete description. This model assumes that after dark halos separate from the Hubble flow and collapse, they subsequently relax to an isothermal sphere of mass M , and the baryons instantaneously settle into a central disk with mass $M_d = m_d M$, where $m_d = \Omega_b / \Omega_0$, Ω_0 is the present-day non-relativistic matter density in units of the critical density, and the baryon density, Ω_b , is set by nucleosynthesis, $\Omega_b = 0.019 h^{-2}$ (Tytler *et al.* 1999). The disk is assumed to have an exponential profile, $\Sigma(R) = \Sigma_0 \exp(-R/R_d)$, with central surface density Σ_0 and scale length R_d , such that $M_d = 2\pi \Sigma_0 R_d^2$. Since the assumptions of a singular isothermal sphere and instantaneous disk formation cannot strictly be true, the apparent success of the model will argue against any strong influence of details such as the profile shape (Mo & Mao 2000) or disk-contraction process on the resultant properties of spirals.

With the gaseous disk in place at the time of formation, star formation proceeds according to an empirical Schmidt law (Kennicutt 1998), such that the star-formation rate (SFR) depends only on the local gas surface density. Given the conservation of baryonic

[†] Most of the freedom in our models comes from the cosmological-parameter choices, which we generally fix to be consistent with current estimates; other choices for these parameters would yield other TF relations, usually inconsistent with the data.

mass, the total SFR, as well as remaining gas fraction, can then be obtained as functions of time since formation by integrating over the disk [see equations (3)–(9) in HJ99]. The model ignores any gas returned to the ISM by stars as well as late infall of fresh gas.

Using the SFR and an assumed stellar initial mass function (IMF), the properties of the stellar populations formed at each time interval are calculated using the spectrophotometric stellar-evolution code of Jimenez *et al.* (1998, 2000), and broad-band magnitudes derived from the resulting spectra are integrated over the life of the galaxy to yield luminosities in various bands. Other stellar-population codes generally yield results which agree to within 0.1–0.2 mag and have comparable dispersions (Jimenez *et al.* 2000). Since we are integrating the SFR over time, weighted by the specific luminosities of model stellar populations as a function of age, metallicity, spin, etc., the model can predict disk luminosities and surface brightnesses (in a variety of wavebands) at any point in their evolution. More details about the calculation of the luminosities of the stellar populations, as well as some possibly useful analytic fitting formulas, are provided in an Appendix.

To summarize, for a given set of cosmological parameters, the model of HJ99 takes as input a total galactic mass, M , and spin, λ , and can output, as functions of time, the disk luminosity and surface brightness in various wavebands, as well as the metallicity.

2.2 Spherical-Collapse Model

We will be interested in the relation between the size and mass of a galactic halo, and this is fixed by the formation redshift—halos of a given mass that undergo collapse earlier are expected to be smaller and denser—through the spherical-collapse model. HJ99 used a simple approximation for the relation between the mass, size, and collapse redshift, neglecting the full impact of a possible cosmological constant. Since our aim is to carefully study the effects of variations in the formation-redshift distribution, we treat the spherical-collapse model more precisely, following the approach of Wang & Steinhardt (1998).

The model will of course depend on the background cosmology, which effectively sets the initial conditions and dictates the course of structure formation. We consider various cold-dark-matter (CDM) models with a power spectrum given by $P(k, z) = AD^2(z)k^n T^2(k)$, where A is the overall amplitude, $D(z)$ is the linear growth factor, and k^n is the primordial power spectrum (we shall assume an untilted, $n = 1$ primordial spectrum throughout). For the transfer function, $T(k)$, we adopt the functional form of Bardeen *et al.* (1986), parameterized by the shape parameter Γ .

We restrict our study to flat geometries ($\Omega_0 + \Omega_\Lambda = 1$, where Ω_Λ is the energy density associated with the cosmological constant, in units of the critical density), and consider various values of h , the Hubble parameter (H_0) in units of $100 \text{ km s}^{-1} \text{ Mpc}^{-1}$. The presence of a cosmological constant introduces several modifications to the standard spherical-collapse model derived for the Einstein-de Sitter case, which are often overlooked. These include a nonzero surface-pressure term in the virial relation, which in turn alters the mass-circular velocity relationship, and introduces Ω_0 -dependent corrections to ρ_{coll} —the density of virialized objects, in units of the present background density, given by a value of ~ 179 at $z = 0$ in the Einstein-de Sitter (EdS) case—and to δ_c , the overdensity ($\delta = \rho/\bar{\rho} - 1$) threshold for collapse, typically taken to be the linearly-extrapolated value of ~ 1.69 in the EdS case (see equations (2), (5), (6), and (7) and related discussion in Wang & Steinhardt 1998). We do not reproduce all of these results, but merely write the equation for the quantity which interests us di-

rectly, namely the circular velocity of the disk, which can be related to the virial velocity of particles in the halo:

$$V_c^2 = \frac{2}{3} \overline{V_{vir}^2} \quad (2)$$

$$\overline{V_{vir}^2} = \frac{3}{5} \left[GMH_0 \sqrt{\Omega_0 \Delta_c / 2} \right]^{2/3} (1+z) \times \left[1 - \frac{2}{\Delta_c} \frac{1 - \Omega_0}{\Omega_0 (1+z)^3} \right],$$

where $\Delta_c = \rho_{coll}/\rho_b$ is the Ω_0 -dependent ratio of the halo to background density at collapse. We stress that these results can, in general, differ substantially from their EdS counterparts.

We incorporate these Λ CDM generalizations into the Press-Schechter (PS) theory, which will be our starting point for calculating halo abundances and formation times. The theory states the familiar result that the comoving number density of halos in a mass interval dM about M at redshift z is given by

$$n(M, z) dM = -\sqrt{\frac{2}{\pi}} \frac{\rho_b}{M} \frac{\delta_c}{\sigma^2(R, z)} \frac{d\sigma(R, z)}{dM} \times \exp \left[-\frac{\delta_c^2}{2\sigma^2(R, z)} \right] dM, \quad (3)$$

where $R^3 = 3M/4\pi\rho_b$, ρ_b is the constant, comoving background matter density, $\sigma(R, z)$ is the rms fractional density perturbation in spheres of radius R , and δ_c is here understood to depend on redshift via an empirically derived relation (L. Wang, private communication).

2.3 Formation-Redshift Distribution

In standard hierarchical models of structure formation, halos of a fixed mass form over a range of redshifts. HJ99 examined only fixed values for the redshift of formation, z_f , for halos, but considered several values to illustrate the effect of a spread in z_f . EL96 performed Monte-Carlo realizations of halo formation histories, using the merger-tree approach (Lacey & Cole 1993, 1994) and a spherical-accretion model, and concluded that the minimum TF scatter resulting solely from the calculated spread in halo formation redshifts is already uncomfortably larger than that observed. They concluded that satisfying the upper limit of a $\sim 10\%$ relative error in velocity dispersion requires that $\Delta z_f/(1+z_f) \lesssim 20\%$. Other workers (e.g., Bullock *et al.* 1999) have looked at the scatter in formation redshifts (or the closely-related scatter in “concentration parameters”) obtained from numerical simulations and found better agreement with the observed scatter.

Although numerical simulations should in principle provide the best way to evaluate the formation-redshift distribution, these have limitations in practice. In particular, it is difficult to collect enough statistics to determine the distributions for different masses and/or to determine how these distributions depend on the cosmological parameters or the power spectrum. As the analytic distributions discussed below demonstrate, it is indeed to be expected that the formation-redshift distribution (and thus resulting scatter in the TF relation) should depend on the mass, cosmological parameters, and power spectrum. Thus, although they can provide some order-of-magnitude estimates, results from numerical simulations can be mis-applied in SAMs if they are determined, say, for one mass from a simulation with a particular choice of cosmology, and then applied to other masses and/or cosmologies. Moreover, analytic methods allow for more obvious and direct insight into the de-

pendence of the model on various parameter choices and assumptions.

Therefore, we follow Viana & Liddle (1996), and explore two plausible analytic models for the distribution of halo formation redshifts. The first, denoted as the ‘S’ distribution, is that of Sasaki (1994), which simply uses the PS formalism to calculate the formation rate of bound objects, weighted by the probability of arriving at some later time without merging, under the assumption that the destruction efficiency is independent of mass. In this model, the distribution of formation redshifts of halos with mass M is given by

$$\frac{dn_S}{dz_f} = -\frac{\delta_c^2}{\sigma^2(R, z_f)} \frac{n(M, z_f)}{\sigma(R, 0)} \frac{d\sigma(R, z_f)}{dz_f}. \quad (4)$$

The S distribution has the advantage of being independent of how one defines a new halo, but the assumption of self-similar merging might be questioned (see, e.g., Percival, Miller & Peacock 2000).

The second distribution, denoted as the ‘LC’ distribution, addressed this shortcoming by employing the merger-tree approach of Lacey & Cole (1993, 1994). In this formalism, halos continually grow with time, and so one must explicitly define the time at which a particular halo has come into existence[‡] (e.g., the epoch of mass doubling). Lacey & Cole (1993) derived expressions for the expected z_f distribution of halos both using analytic counting arguments and a Monte-Carlo approach to generate merger histories for $M(t)$ explicitly. They found that the former approach yielded excellent agreement with N -body results, while the latter overestimated halo ages (Lacey & Cole 1994). Their results did not depend strongly on the value of the local slope of the power spectrum. The z_f distribution in this model is given by

$$\frac{dn_{LC}}{dz_f} = p(w(z_f)) \frac{dw(z_f)}{dz_f}, \quad (5)$$

where

$$p(w(z_f)) = 2w(z_f)(f^{-1} - 1)\text{erfc}\left(\frac{w(z_f)}{\sqrt{2}}\right) - \sqrt{\frac{2}{\pi}}(f^{-1} - 2)\exp\left(-\frac{w^2(z_f)}{2}\right), \quad (6)$$

$$w(z_f) = \frac{\delta_c(\sigma(M, 0)/\sigma(M, z_f) - 1)}{\sqrt{\sigma^2(fM, 0) - \sigma^2(M, 0)}}, \quad (7)$$

and f is the fraction of halo mass assembled by formation redshift z_f . Thus at fixed redshift, models with higher values of f produce younger galaxies. Lacey & Cole adopted $f = 0.5$, identifying the mass doubling epoch as the nominal point at which halos are born, while Viana & Liddle (1996), looking specifically at the mass-temperature relation for galaxy clusters, use a value of $f = 0.75$. Note that in any of these models, the dependence on the power spectrum is only through $\sigma(M)$, the rms fractional density perturbation for the mass scale M ; the dependence on Ω_0 and h

[‡] This ambiguity arises because in the excursion-set formalism, one follows a random walk of trajectories of the spatially-filtered δ to the first up-crossing above some threshold value. The ‘‘tagged’’ mass is statistically defined as the expectation value for the mass of a halo in which a given particle will end up, but this will in general differ from the actual mass in a given realization. This ambiguity can lead to predictions of negative probability densities at $z \sim 0$ in models with primordial power-spectrum indices $n > 0$.

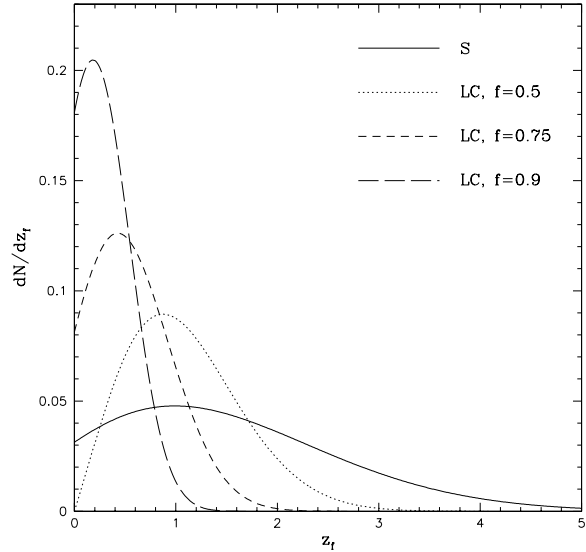


Figure 1. Formation-redshift distribution for the S distribution (solid line) and for the LC distribution with $f = 0.5, 0.75,$ and 0.9 (dotted, short-dashed, and long-dashed lines, respectively), assuming a Λ CDM model with $\Omega_0 = 0.3$ and $h = 0.65$. Note the appreciable width of the S distribution, and the decreasing width and peak z_f values for LC distributions with increasing f .

enter through the linear-theory growth factor and in the spherical-collapse physics, and through the star-formation model by fixing ages, baryon fraction, etc.

Figure 1 depicts the distribution of formation redshifts for halos of $10^{12} M_\odot$ both for the S distribution, and for the LC distribution with f values of 0.5, 0.75, and 0.9 for comparison. These results assume a COBE-normalized Λ CDM model with $\Omega_0 = 0.3$ and $h = 0.65$ (yielding, in this case, a mean peak height of $\nu = 0.69$, and $\sigma_8 = 1.08$). Note the large width of the S distribution, peaking at $z \sim 1.0$, but with a significant tail extending out to $z \sim 4-5$, and appreciable ongoing formation today[§]. By contrast, LC distributions with larger values of f produce much narrower distributions which peak at lower redshifts and fall more rapidly to high z .

2.4 Spin Distributions

Assuming constant specific angular momentum, the disk scale length can be related to λ , the spin parameter of the halo (e.g., Mo, Mao, & White 1998),

$$R_d = \frac{\lambda GM}{\sqrt{2}V_c^2}, \quad (8)$$

fixing the initial surface density of the gas and thus affecting the SFR, luminosity, and surface brightness. Therefore, it might be supposed that the predicted TF relation and other properties would depend sensitively on spin. HJ99 considered only fixed values for λ , rather than accounting for its detailed distribution. The spin distribution is usually taken to be a log-normal centered at $\lambda \sim 0.5$,

[§] This long tail will disappear if one uses the formalism developed in Percival, Miller & Peacock 2000

as indicated by numerical simulations. However, as is the case for the formation-redshift distribution, heuristic arguments suggest that the distribution of spin parameters should depend on the mass, the formation redshift, and possibly on the cosmological parameters and/or power spectrum. If so, the effect of scatter in the spin parameter on the TF relation could be different than that inferred from numerical simulations.

Heavens & Peacock (1988) calculated the distribution of tidal torques acting on matter in the vicinity of mildly nonlinear density maxima, assuming a spherical-accretion model to calculate binding energies, and derived the resulting spin-parameter distribution. They found an anti-correlation between peak height and spin parameter, but pointed out that the intrinsically broad range of the λ distribution swamped the systematic shift with peak height, ν , resulting in a fairly weak anti-correlation. Catelan & Theuns (1996) extended these results to obtain the joint PDF for spin parameters and peak masses using the distribution of peak shapes in different CDM models. They confirmed the broadness of the spin-parameter distribution, and the anti-correlation with peak height (which owes essentially to the fact that higher peaks will generally be more spherical, and thus harder to spin up). Their results, however, exhibit a systematic shift toward higher λ values than those of Heavens & Peacock, such that $\nu = 1$ peaks have rms λ values of ~ 0.15 , instead of 0.05, thus closer to the observed value of 0.5 for spirals. The anticorrelation conjecture has not been fully tested by simulations, but some support comes from Ueda *et al.* (1994). Lemson & Kauffmann (1999) argued against an environment-dependent λ . However, the environment was defined on a $10 h^{-1}$ Mpc scale, and we do not expect strong correlation between the density field smoothed on galaxy scales and this large scale.

Since the indications for a distribution peaked at higher spins and an anti-correlation with peak height are good, but not yet well-established, we consider two models, with and without the joint distribution in λ and ν . For the former, we adopt the joint distribution function (Catelan & Theuns 1996),

$$P(\lambda|\nu) = \frac{0.68}{\lambda} \left[1 + 0.02 \left(\frac{\lambda}{\lambda_0(\nu)} \right)^4 \right] \times \exp \left[-\frac{\log^2(\lambda/\lambda_0(\nu))}{0.98} \right], \quad (9)$$

where $\lambda_0(\nu) = 0.11\nu^{-1.1}$ and $\nu = \nu(z) = \delta_c(z)/\sigma(R, z)$. Since, at a fixed epoch, there is not a one-to-one relationship between ν (defined for the spatially averaged overdensity field) and mass, owing to the distribution of halo shapes, equation (12) effectively corresponds to an average of ν over all shapes of a given mass. ¶

2.5 Chemical Evolution

HJ99 assumed the stellar populations to have constant metallicity fixed at the solar value for all time. More realistic models should, of course, account for chemical evolution. To study the effect of

¶ We point out that the binding energy used to calculate λ is derived using a spherical-accretion model, but that for the lower, more irregular peaks, this is likely only a lower limit to the actual binding energy, resulting in an underestimate of λ . Combined with the arguments above from Catelan & Theuns (1996), one can push the predicted spin values for spirals (if these are indeed associated with lower- ν peaks, as opposed to ellipticals, which are associated with higher peaks) closer to the observed values, such that one needn't rely as heavily on dissipation to spin up spirals.

chemical evolution on the TF relation, we assume that galaxies are (chemically) closed boxes, for which analytic results for the evolution of metallicity exist (e.g., Pagel 1997). This assumption seems to be justified by the detailed hydrodynamical computations of a multi-phase ISM by Mac Low & Ferrara (1999). In order to relax the instantaneous recycling approximation we adopt a value of 0.03 for the yield in order to account for the delayed production of Fe by Type-Ia supernovae. We also set the zero-point redshift dependence so as to comply with observations of damped Lyman- α systems, which suggest that the ISM is already enriched up to a certain metallicity at a given redshift. Adopting the relation derived by Pettini *et al.* (1999; see Figure 8 therein), we have that the metallicity, Z , evolves with redshift, z , as

$$Z(z, z_f) = 0.03Z_\odot \ln \left(\frac{1}{f_g(z, z_f)} \right) + 0.28Z_\odot 10^{-0.25z}, \quad (10)$$

where the solar metallicity $Z_\odot = 0.02$ and $f_g(z, z_f)$ is gas fraction of the disk. It will be shown that chemical evolution will be an important factor in reducing the predicted scatter in the TF relation.

3 RESULTS

We first study the respective impacts of the various ingredients which have entered into our galaxy-formation model. In Figures 2 to 12, we illustrate examples of how our predictions for the TF relation in the B , R , I , and K bands change as the model inputs are varied. These results will allow the reader to infer how the predictions of any of our models, or any other models that appear in the literature, would change with different input physics or assumptions. In each graph, the solid line delineates the power-law fit to the TF-relation prediction (along with $1-\sigma$ errors given by the dashed lines, and denoted in each plot by ‘ σ ’), and the four scattered-dot curves trace the spread in the predicted TF relation for four fixed masses (10^{10} , 10^{11} , 10^{12} , and $10^{13} M_\odot$), using ~ 150 points each.

Overplotted on each graph are open symbols representing data from Tully *et al.* (1998). These data, comprised of spiral galaxies in the loose clusters of Ursa Major and Pisces, represent one of the most carefully defined TF samples. The inclination-corrected FWHM of the lines has been converted to W_R^i , which approximates to $2V_c$, and the data have been corrected for dust extinction. The scatter in the B , R , I , and K bands is 0.50, 0.41, 0.40, and 0.41 mag, respectively. While many authors compare their models to TF data by defining a “fundamental” TF relation derived from the particular data set in question, we argue that, given the observational selection effects inherent in defining such samples, there is no particular significance or accuracy associated with any one determination of the slope and normalization of the TF relation. Instead, we examine how well these data fit to our model, in a χ^2 sense, using the measured scatter as an estimate of the error associated with each point. For each plot we calculate the resulting χ^2 and denote by ‘ p ’ the probability of obtaining this large a value of χ^2 given that the model is correct; values of p below 10^{-3} are listed as zero. In addition, since the data have excluded spirals which show evidence of merger activity or disruption in the form of starbursts, we exclude from our model galaxies those having $B - R < 0.3$.

3.1 Formation-Redshift Distribution

3.1.1 S Distribution

As discussed above, the distribution of formation redshifts should lead to some scatter about the TF relation, and Figure 2 illustrates this effect using the S distribution. We show results for two cosmogonies to indicate the dependence of the results on some of the cosmological parameters. The left-hand panels of Figure 2 depict the results for the S distribution of z_f in an EdS universe, while the right-hand panels show the results for a flat, Λ -dominated universe. Here, and unless otherwise indicated, we shall take EdS models to have $h = 0.65$, a power-spectrum shape parameter^{||} $\Gamma = 0.2$, and an rms density contrast fluctuation over $8h^{-1}$ Mpc spheres of $\sigma_8 = 0.5$. For Λ CDM models, we assume $\Omega_0 = 0.3$, $h = 0.65$, a COBE-normalized power spectrum (Bunn & White 1997) with $\Gamma = \Omega_0 h = 0.195$, and for all cosmogonies we assume $\lambda = 0.05$, a fixed metallicity given by the solar value ($Z = Z_\odot$), and a Salpeter IMF, $d \log N_*/d \log M_* = -\alpha$ with $\alpha = 1.35$, all unless otherwise indicated.

To understand the results, we begin by examining the predictions for the K -band TF relation in the Λ CDM model. Here we find that the spread in z_f translates directly into a spread in V_c (with earlier formation implying higher circular velocity) which widens for lower masses, since these can form over a broader range of redshifts stretching back to higher z . This broadening of the TF with lower V_c arises generically from a realistic formation-distribution, and it is observed in most TF samples. The predicted M_K , however, varies very little for galaxies of a given mass, since this wavelength primarily traces the older stellar population. In general for our models, the distribution in z_f is found to be the primary source of scatter in the TF relation.

As we go to bluer bands, we find that for a given mass, younger galaxies become brighter, increasing the spread in the TF relation. This is a simple consequence of equation (8) in HJ99, which states that the SFR is a rapidly declining function of age. There is a competing effect, however, from the fact that galaxies that are too young will not have had enough time to convert much gas into stars, and so will become dimmer. For this reason, our plots often outline a peak magnitude for galaxies of a given mass, in those cases where the z_f distribution produces a large fraction of very young galaxies. Such galaxies would likely exhibit the properties of starbursts and be excluded from carefully-defined TF samples. Indeed, model galaxies removed by our color selection criterion ($B - R < 0.3$) tend to be those on the younger side of these peaks.

Overall, these S distribution predictions do not fit the TF data in any waveband, as the models are too faint in every case, and the predicted scatter here is too large by about 0.7 mag in B and 0.3 mag in K . The problem owes largely to the fact that the S distribution has a substantial high-redshift tail producing older, fainter galaxies with high V_c . Thus, if we assume star formation proceeds according to a Schmidt law, TF observations imply that *the majority of present-day disks could not have formed much beyond a redshift of 2–3*.

^{||} Since values of $\Omega_0 h \gtrsim 0.3$ already seem to be ruled out (e.g., Peacock & Dodds 1994), Γ in the case of EdS models is defined simply as a fitting parameter in the CDM transfer function. In the case of Λ CDM models, we formally take $\Gamma = \Omega_0 h$.

3.1.2 LC Distribution

Figure 3 depicts corresponding results for the same parameter choices, but using the LC distribution with $f = 0.75$. This distribution has both a lower peak value of z_f and a smaller FWHM than the S distribution (see Figure 1), producing significantly less scatter in the predicted TF relations and a larger fraction of younger galaxies, as compared with Figure 2. Despite the smaller scatter, these models still do not fit the observed TF relation in the various bands. Note that the EdS model here actually yields excellent agreement in B , but predicts galaxies which are too faint in I and K .

In Figures 4 and 5 we examine LC distributions with values of $f = 0.5$ and $f = 0.9$, respectively. Lacey & Cole (1993, 1994) found that the statistics of the time at which present-day halos accreted half their mass (i.e., $f = 0.5$) provides an excellent fit to the results of N -body simulations. Here we see that the $f = 0.5$ Λ CDM model provides an excellent fit to the K -, R -, and I -band TF relations but predicts galaxies which are too faint in B , thus highlighting the importance of using multi-wavelength constraints. This model also produces TF scatter which is about 0.1 to 0.4 mag too large, going from K to B . The EdS predictions here have less scatter, but are again too faint in every case. In general, we find that LC distributions with plausible values of f fare better than S distributions at matching TF data, suggesting disk formation in the range $0 < z < 2$ (see below).

The $f = 0.9$ models have a z_f distribution which produces galaxies only in a narrow interval centered at low redshift (see Figure 1). This results in extremely small TF scatter in part because effectively no galaxies form above a relatively low maximum redshift of $z \sim 1$, but also because many of these recently formed galaxies fall on the young side of the magnitude peak and are excluded by our color selection. In effect, this z_f distribution has “pushed” galaxies over to the faint side of the magnitude peak, where their colors resemble those of starbursts, and the low scatter owes to the small number of galaxies “older” than the peak, particularly in K . Thus, while the intrinsic TF scatter of all galaxies in this model is high, the observed scatter, based on observational selection, can be quite low, and this effect is important when considering recently formed populations.

Irrespective of the scatter, however, the $f = 0.9$ models fail to fit the TF slope and normalization. For the reasonable cosmological-parameter values in the right panels, the predicted galaxies are very young and thus excessively bright. Thus, TF constraints also imply that *the majority of disk formation cannot have happened at $z < 1$* . Of course, from a physical standpoint, such large values of f are anyway unreasonable. Note that even with $f = 0.9$, the EdS model still produces galaxies which are too faint in K , despite yielding excellent agreement in I .

3.2 Dependence on Cosmogony

3.2.1 Power-Spectrum Shape and Amplitude

In Figure 6 we explore the impact of individually changing the shape and normalization of the power spectrum, using the S distribution in an EdS universe. In the left (right) panels we adopt $\Gamma = 0.5$ ($\Gamma = 0.2$) and $\sigma_8 = 0.5$ ($\sigma_8 = 1.0$). In both cases, the resulting galaxies are several magnitudes too faint and produce dramatically larger scatter in their TF relation. In the case of higher σ_8 , halos of a given mass will be smaller, and correspond to rarer peaks. These collapse at earlier times, leading to larger V_c and older, dimmer galaxies. Extending the range of collapse redshifts

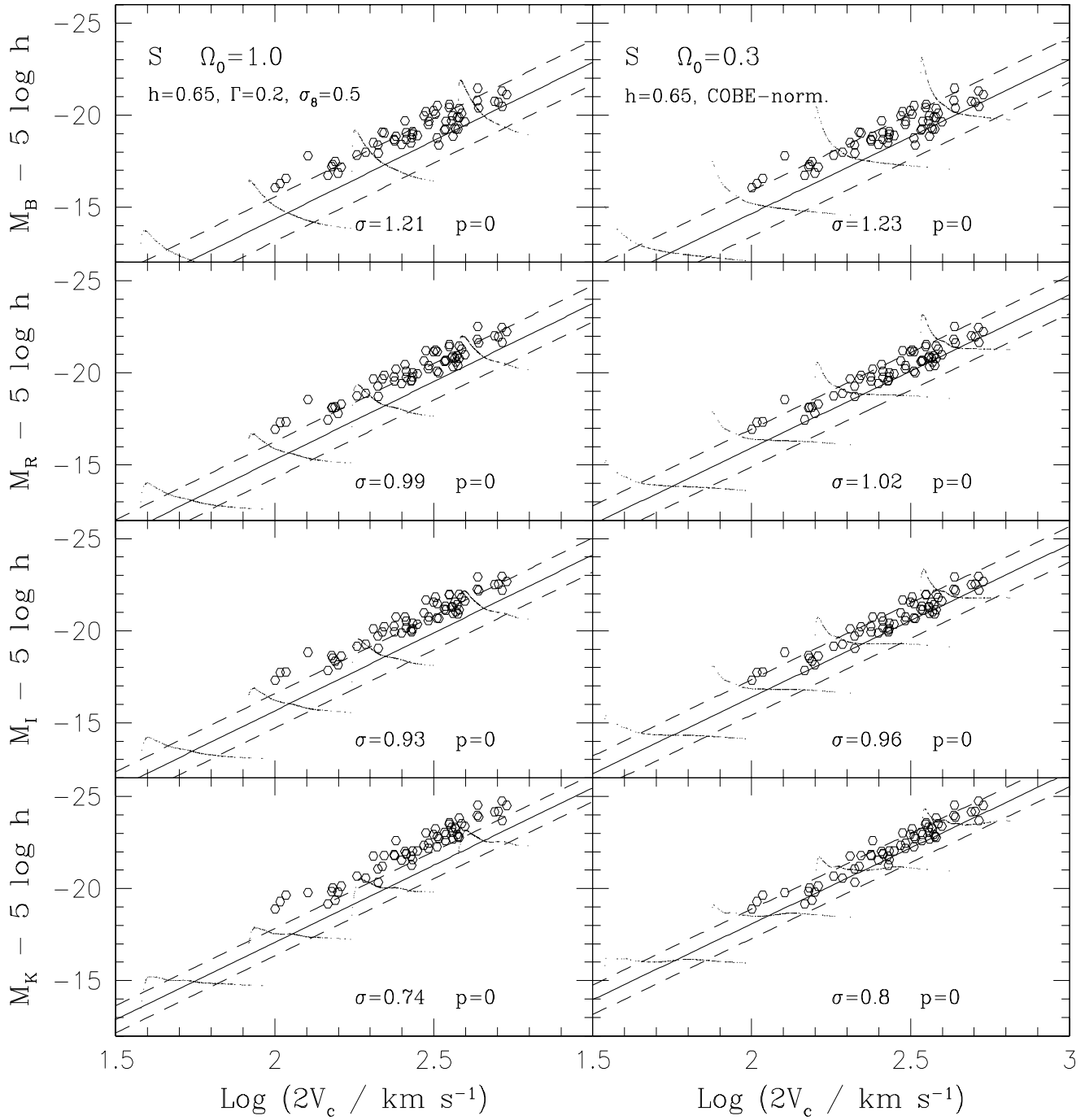


Figure 2. S-distribution predictions. The left panels show the predictions for the present-day TF relation in B , R , I , and K for the S distribution assuming an EdS universe with $h = 0.65$ and a CDM power spectrum with $\Gamma = 0.2$ and $\sigma_8 = 0.5$. The right panels display the results for a COBE-normalized Λ CDM model with $\Omega_0 = 0.3$, $h = 0.65$, and $\Gamma = \Omega_0 h$. Both assume a Salpeter IMF, a constant spin parameter of $\lambda = 0.05$, and constant metallicity fixed at the solar value. The model predictions for halos of mass 10^{10} , 10^{11} , 10^{12} , and $10^{13} M_\odot$ are indicated by the four scatter-point curves in each panel, and the solid lines are the fits to these predictions, with $1\text{-}\sigma$ errors indicated by the dashed lines. The open symbols are data from Tully *et al.* (1998). Note the EdS model, in particular, underpredicts the luminosity in all bands.

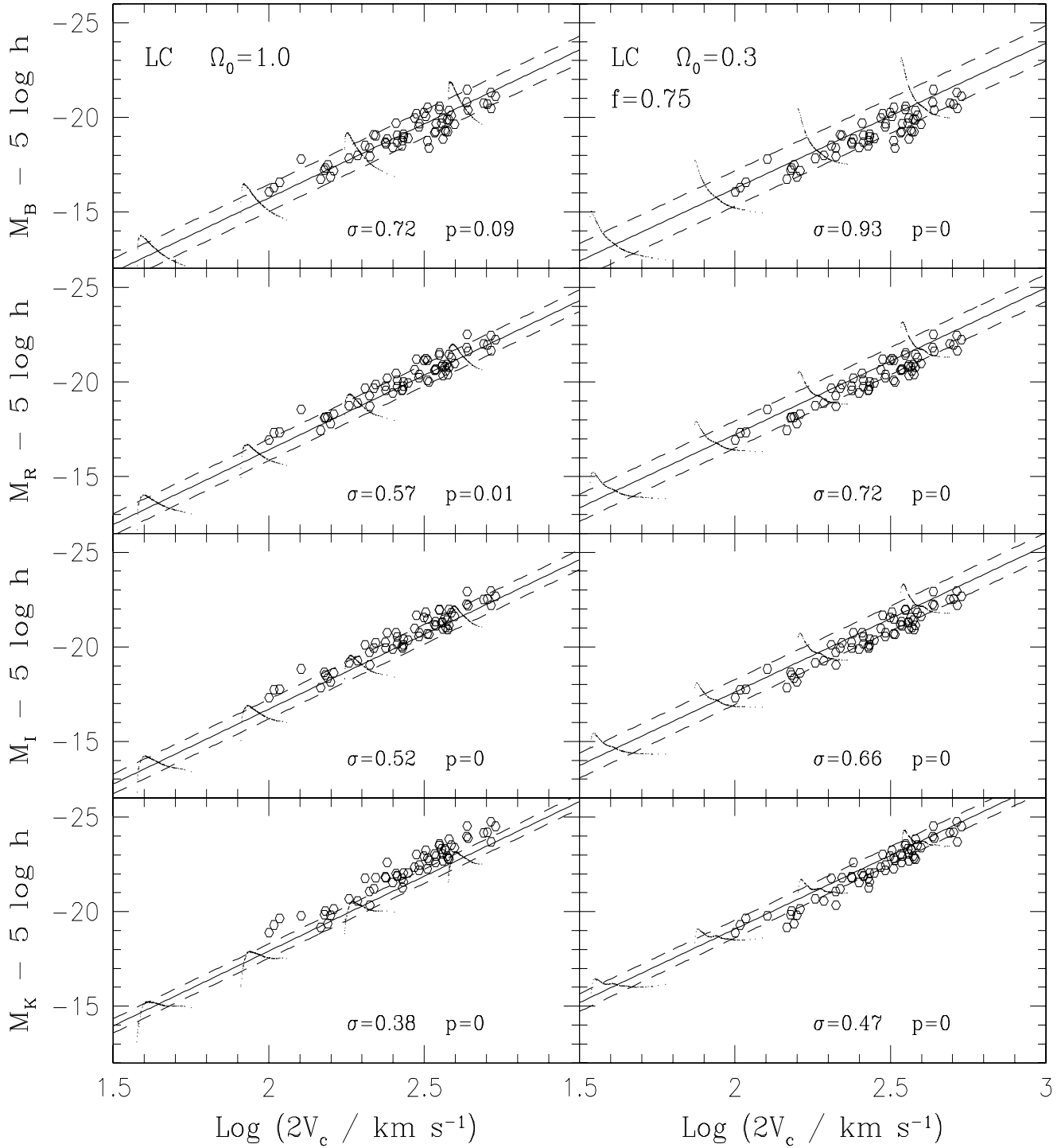


Figure 3. LC-distribution predictions. Same as Figure 2, but using the LC distribution with $f = 0.75$.

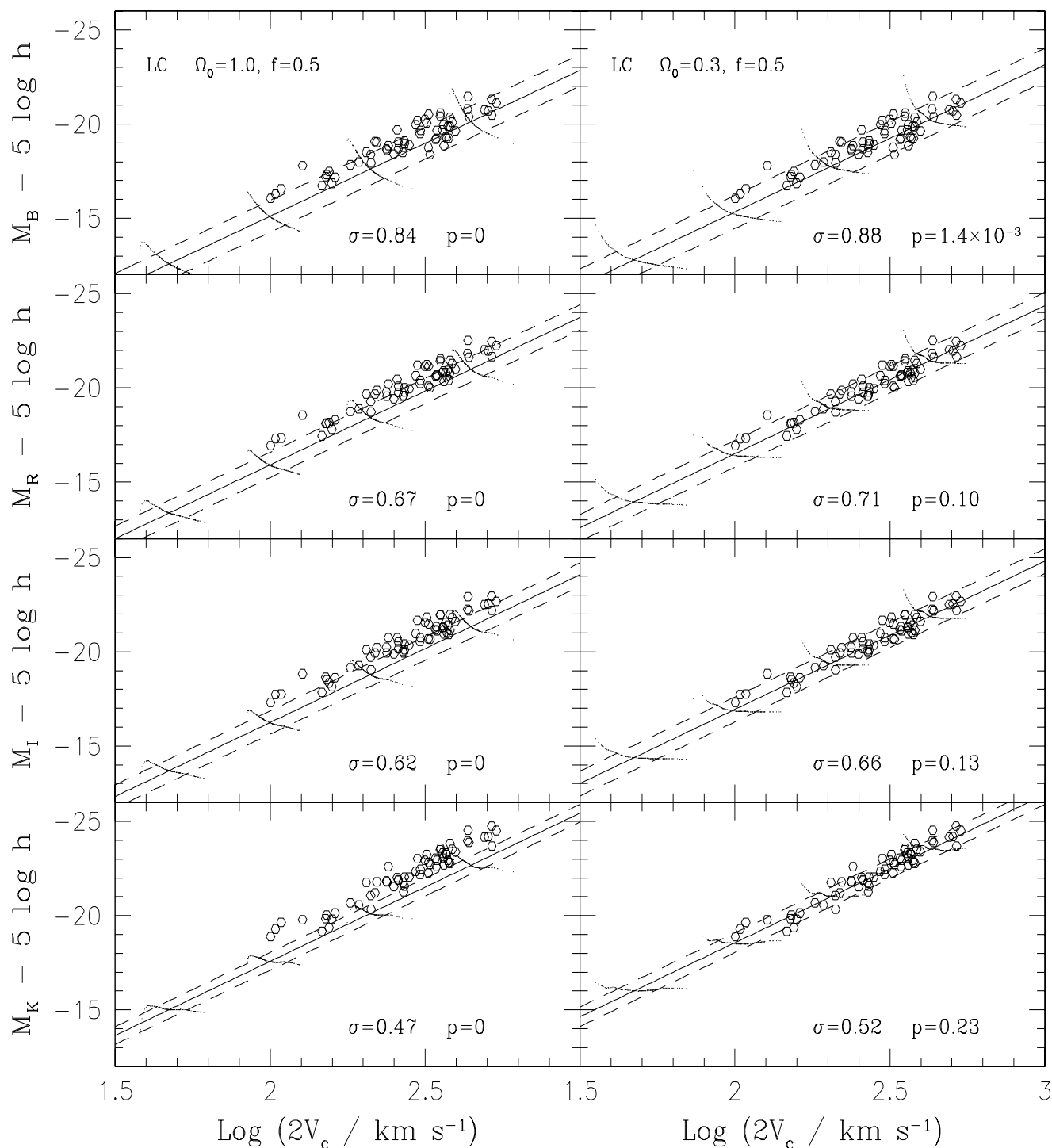


Figure 4. Same as Figure 3, but using $f = 0.5$. Note how the Λ model yields excellent agreement in K , R , and I , but provides a relatively poorer fit in B .

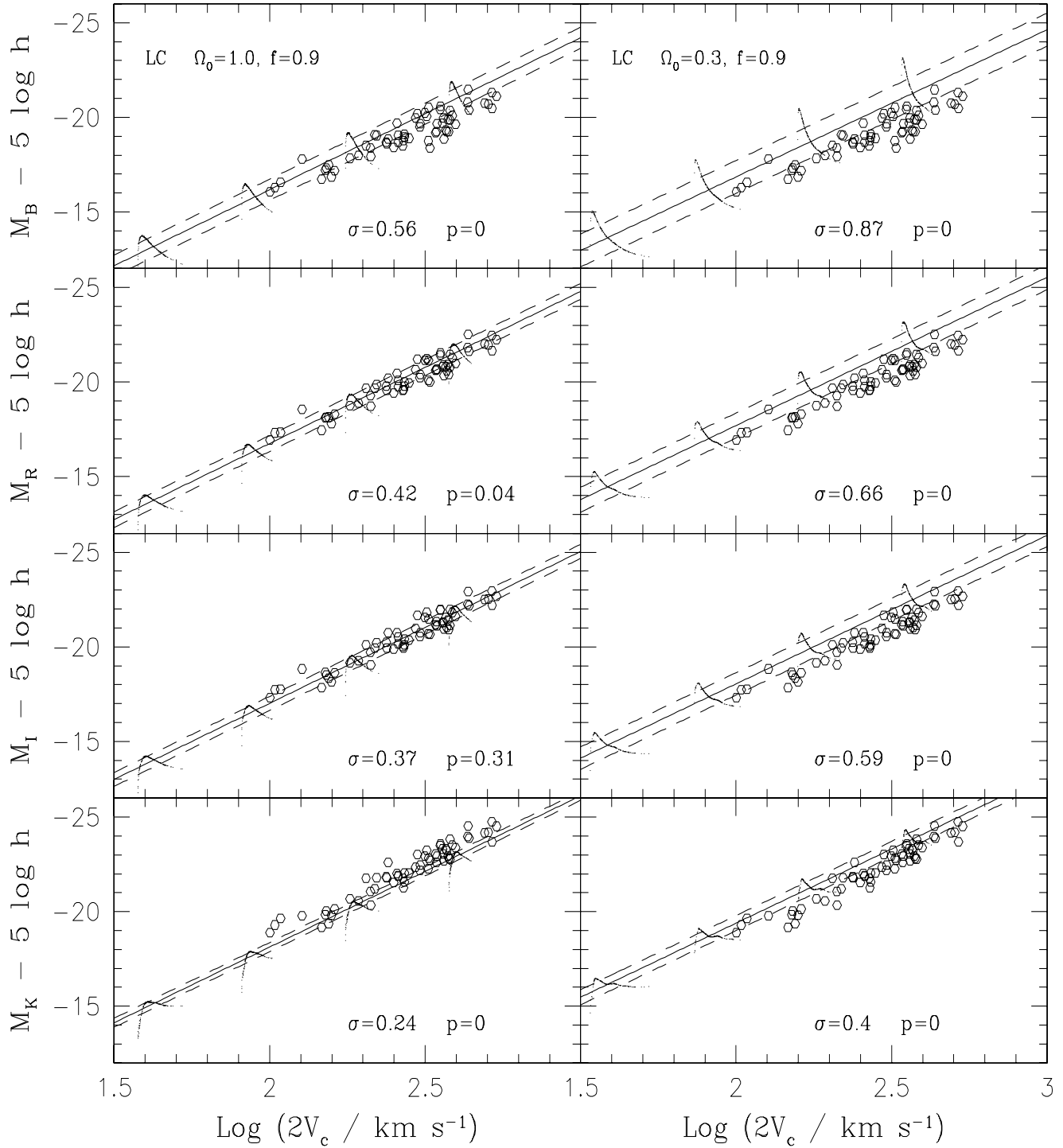


Figure 5. Same as Figure 3, but using $f = 0.9$. In this case, all disks form very recently and many fall on the younger side of the magnitude peak. These effects combine to yield very little TF scatter for the few relatively older galaxies which fall red-ward of our color selection criterion. The overall agreement however, is poor.

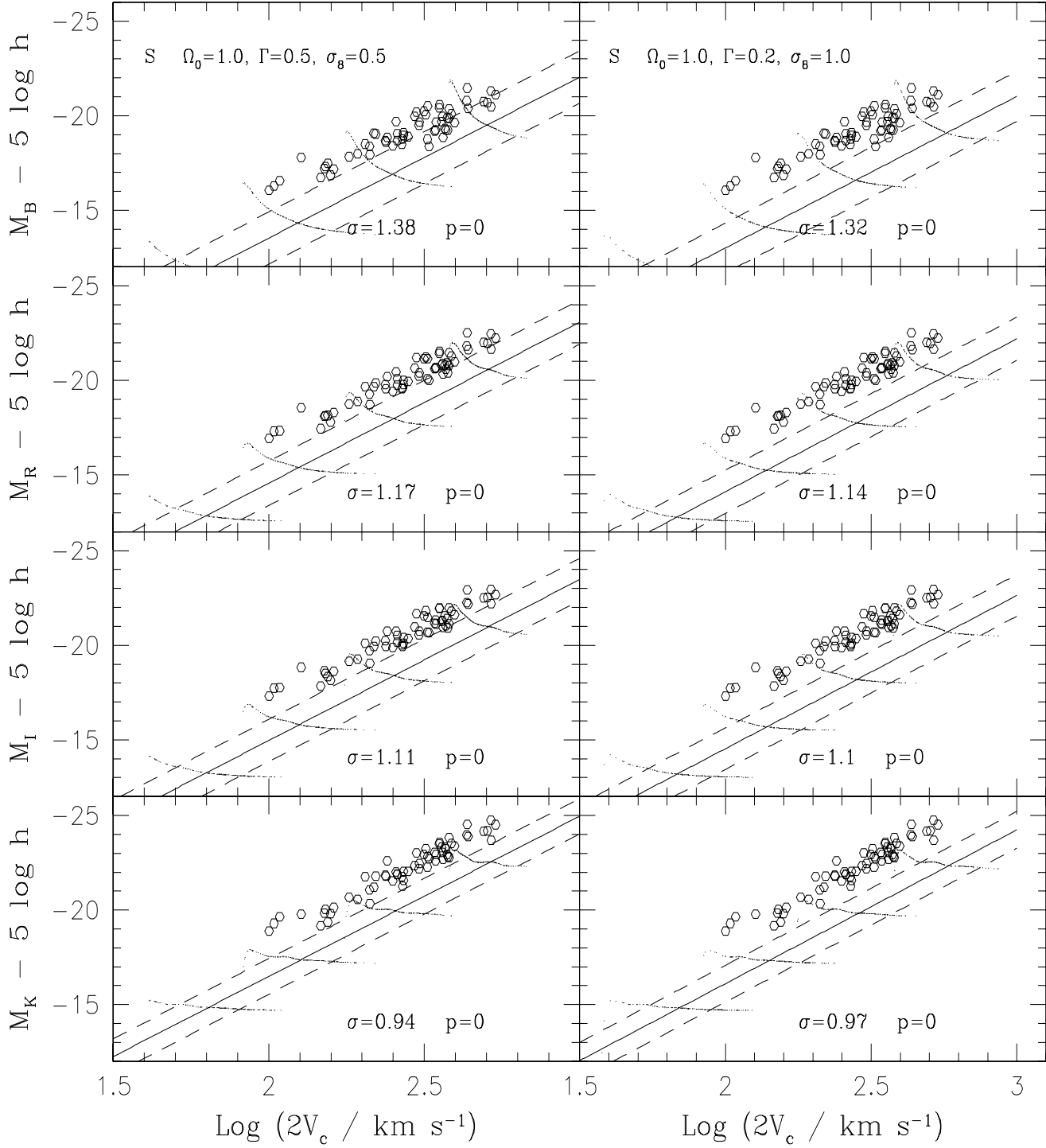


Figure 6. Dependence on the power spectrum shape and amplitude. TF predictions for the S distribution in an EdS universe for $\Gamma = 0.5$ and $\sigma_8 = 0.5$ (left panels), and for $\Gamma = 0.2$ and $\sigma_8 = 1.0$ (right panels). Comparing with Figure 2, we find that high Γ and high σ_8 both lead to earlier collapse, producing fainter disks with a much larger TF scatter.

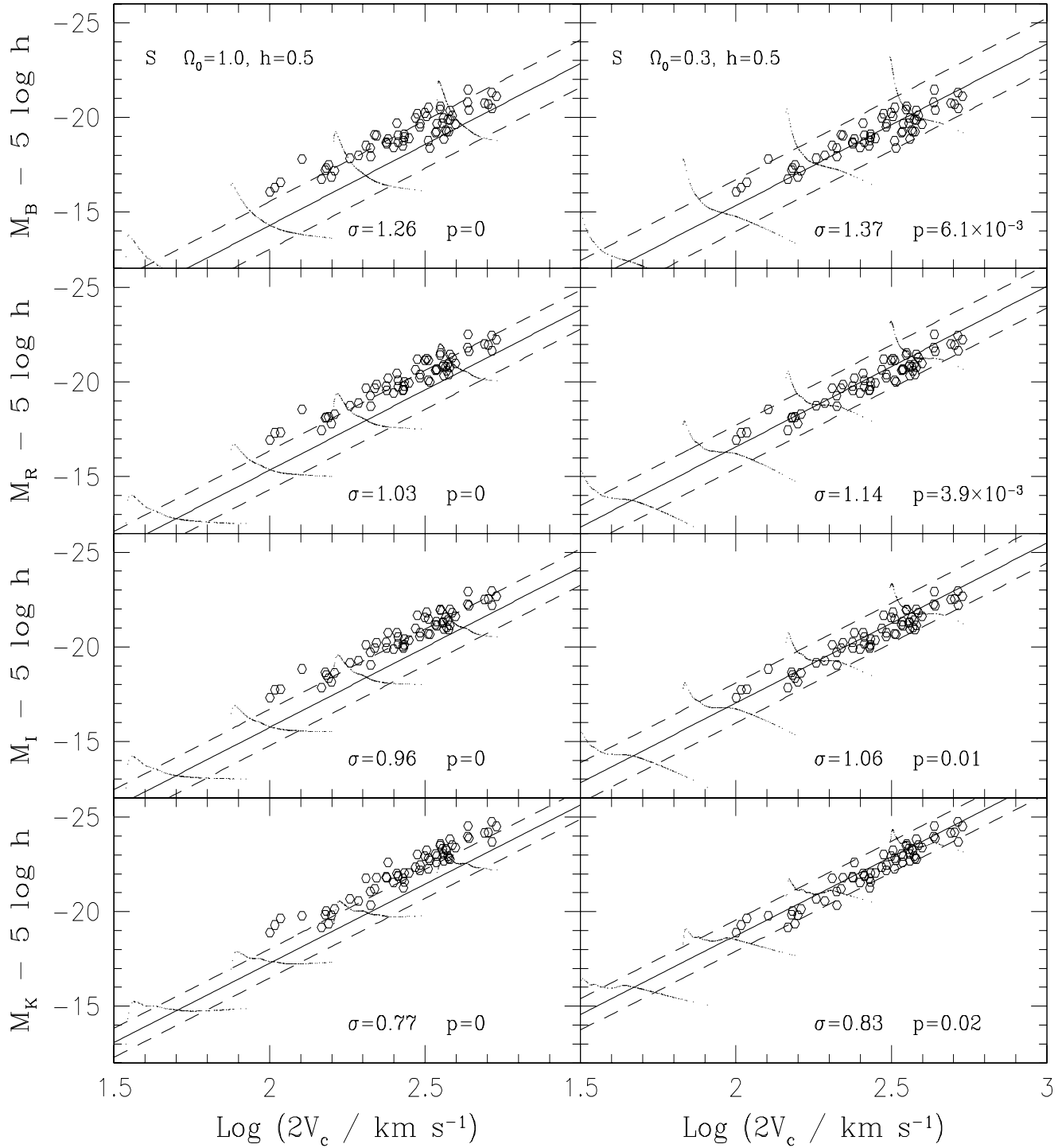
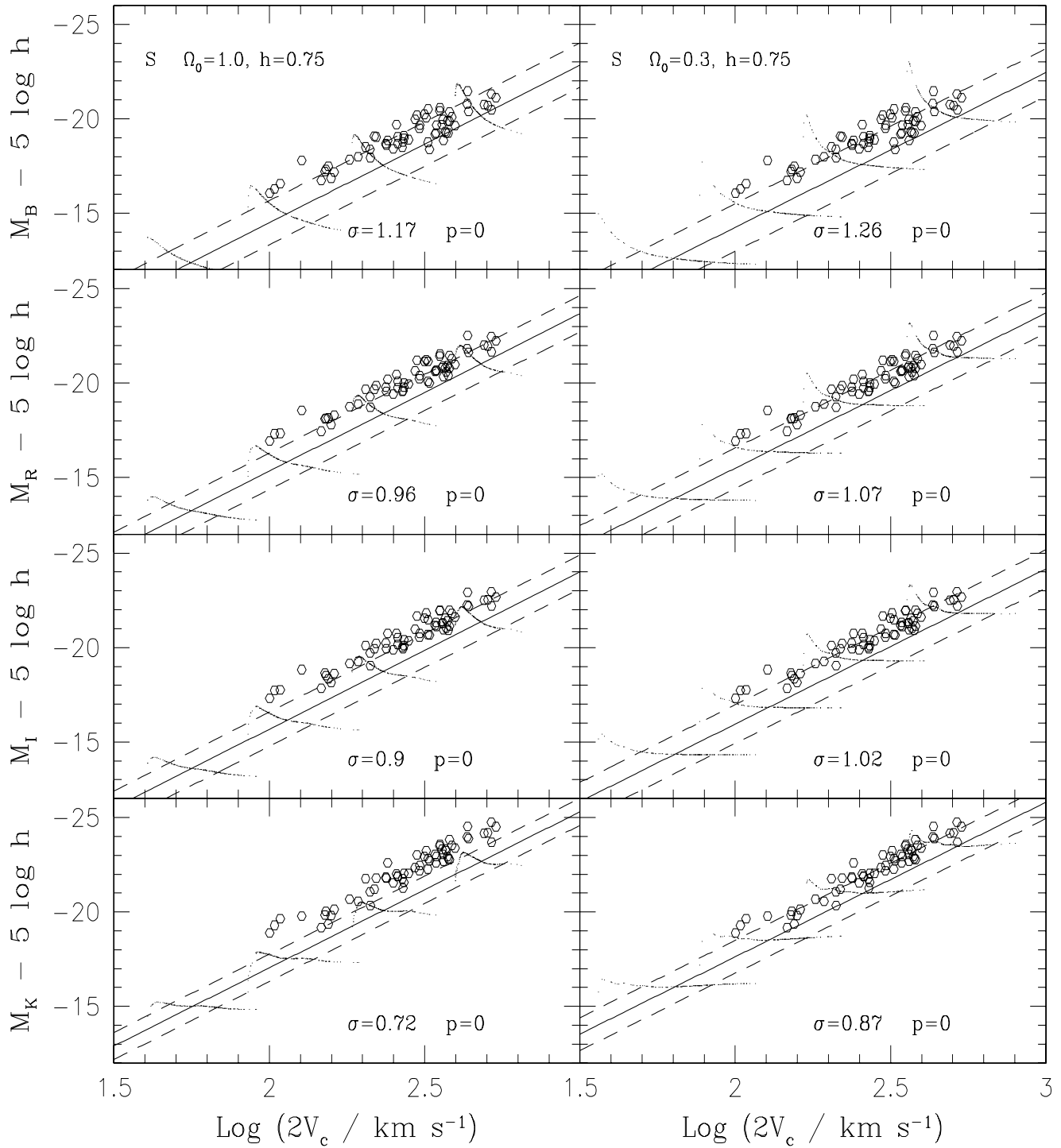


Figure 7. Dependence on the Hubble constant. Same as Figure 2, but using $h = 0.5$. The resulting changes in baryon fraction and age lead to a brightening of the TF relation, particularly for low Ω_0 .

Figure 8. Same as Figure 2, but using $h = 0.75$.

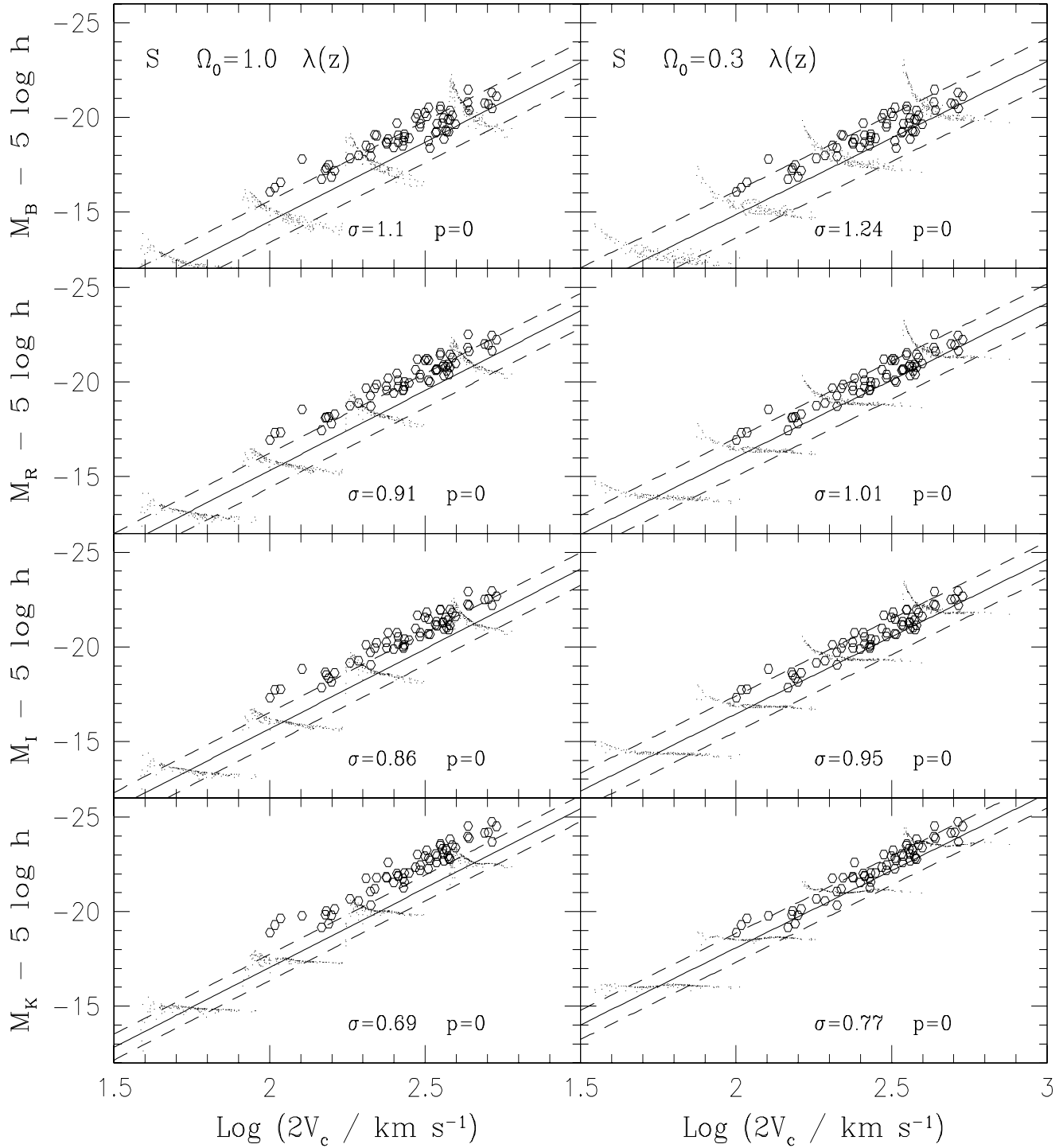


Figure 9. Effect of joint distribution in spin and peak height. Same as Figure 2, but now incorporating both the predicted shape of the spin-parameter distribution and the anti-correlation between spin and peak height. These results differ little from those of Figure 2; the joint distribution in λ and ν scatters the predictions, by a small amount, along the TF relation itself, tightening the TF relation in some cases.

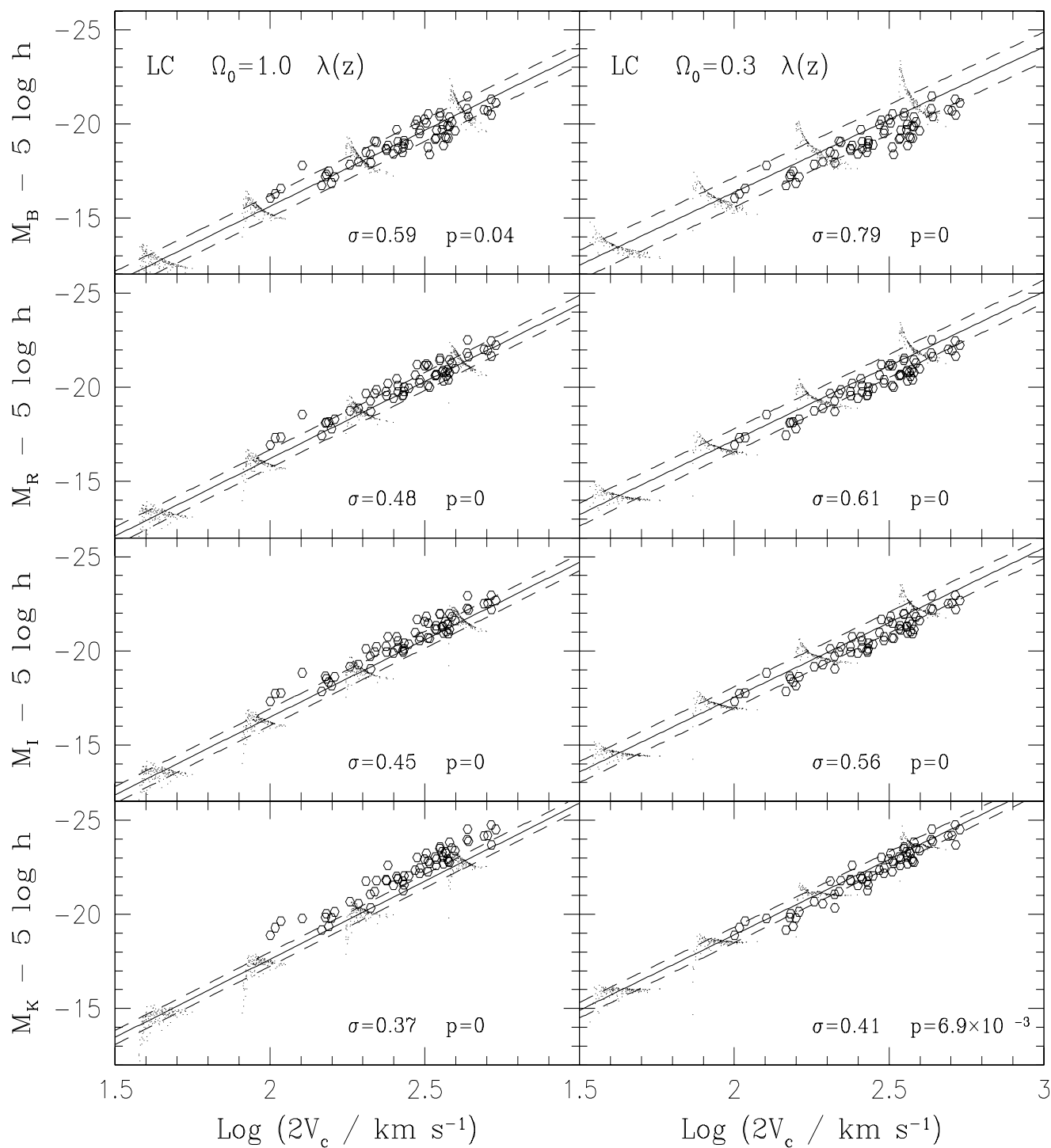


Figure 10. Same as Figure 3, but now incorporating the joint PDF in λ and ν into the LC results.

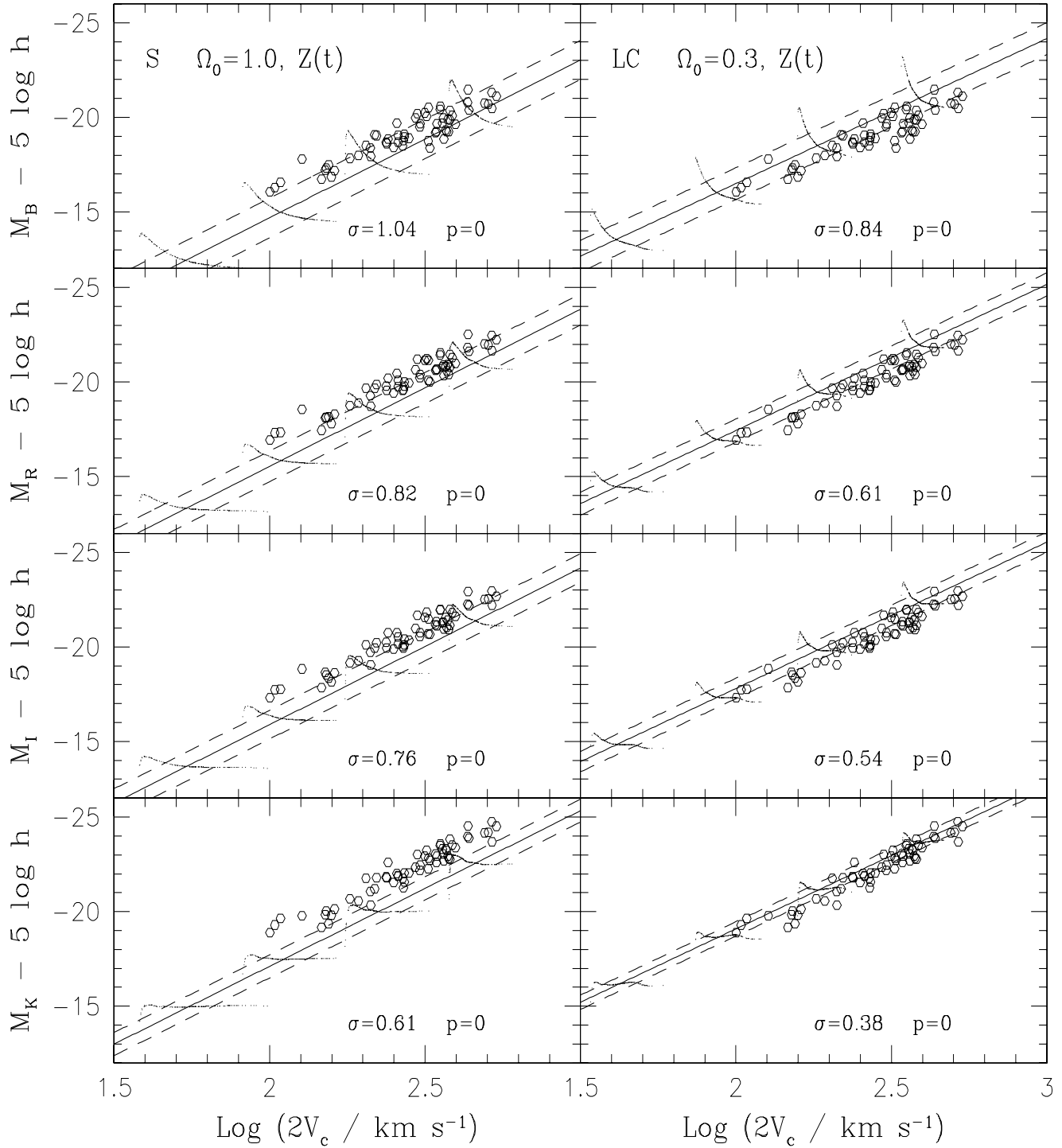


Figure 11. Effect of chemical evolution. TF predictions for an $\Omega_0 = 1$ S distribution (left panels) and an $f = 0.75$ LC distribution with $\Omega_0 = 0.3$ (right panels), both with evolving metallicity. Note the smaller TF scatter as compared to the corresponding results in Figures 2 and 3.

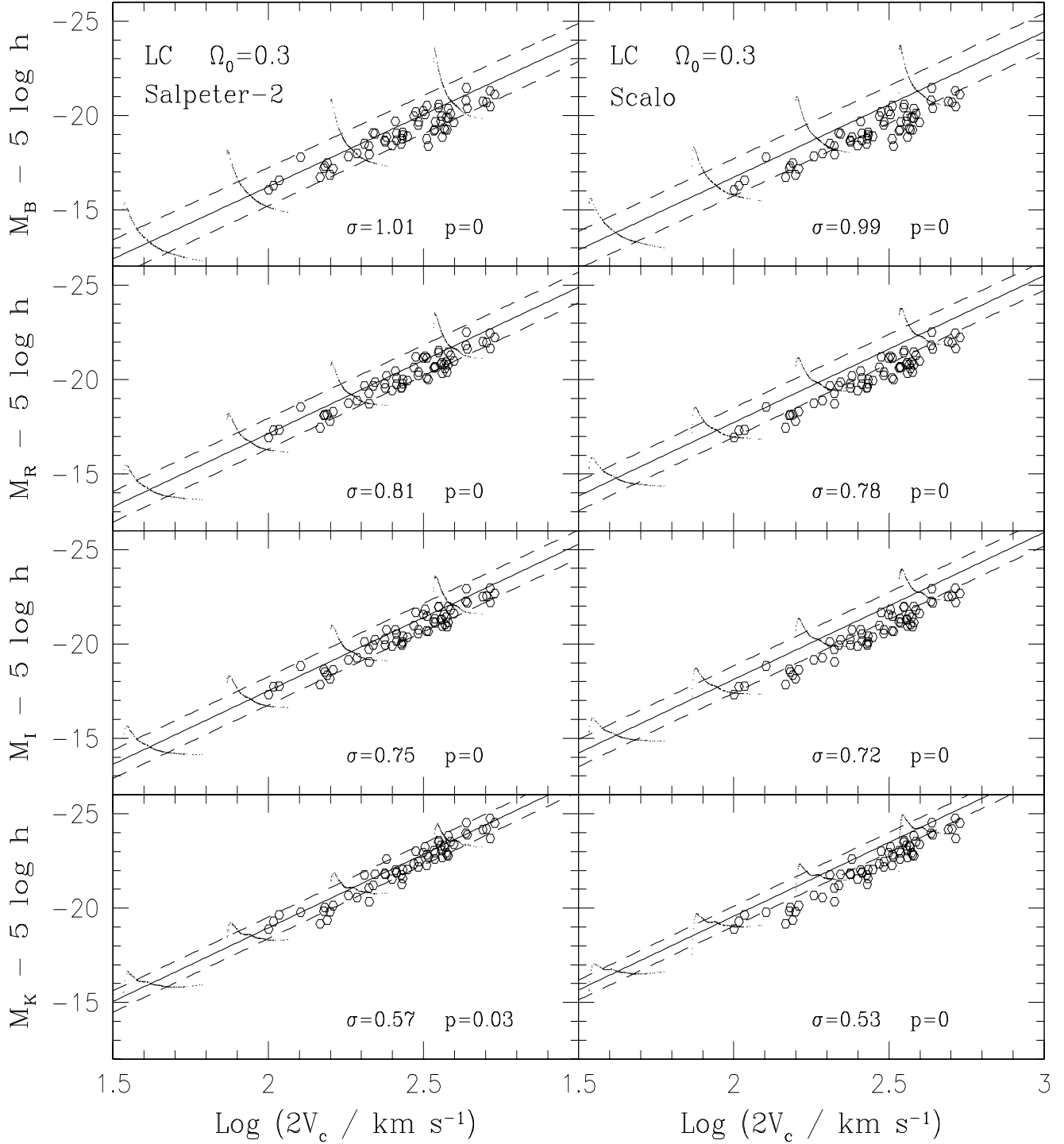


Figure 12. Dependence on the IMF TF predictions for an $f = 0.75$ LC distribution with $\Omega_0 = 0.3$, assuming a Salpeter IMF with index $\alpha = 0.95$ (left panels), and a Scalo IMF (right panels). These IMFs produce relatively more massive stars than the $\alpha = 1.35$ Salpeter IMF investigated previously, and thus brighter TF predictions than those in the right panels of Figure 3.

back to higher z also substantially increases the scatter. Similarly, in these Λ CDM models, increasing Γ shifts more power to smaller scales ($R \lesssim 10$ Mpc), leading to the same result. Though we do not explicitly explore variations with n , it can be inferred that values of $n > 1$, which also tilt power towards smaller scales, will have a similar effect. Conversely, values below unity might lead to better agreement with the data, but there are already strong constraints on the tilt (e.g., Kamionkowski & Buchalter 2000).

3.2.2 Hubble Constant and Matter Density

Given the uncertainties in our present understanding of galaxy formation, it makes little sense to attempt to constrain cosmological parameters using TF data. Rather, with these parameter values dictated by other, more direct tests, we should employ the TF relation to gain insight into these details. Variations in Ω_0 and h affect almost every aspect of the model, such as the disk mass fraction, galaxy ages and circular velocities, star-formation rates, and the power-spectrum shape. In Figures 7 and 8 we plot S distributions with $h = 0.5$ and $h = 0.75$, respectively. Little change is seen in the EdS cases, while for low Ω_0 the net result appears to be that lower (higher) values of h produce galaxies which are brighter (fainter). Changes in h do not, however, strongly affect the scatter. Note that the $h = 0.5$ Λ CDM model provides reasonable agreement in K and I , but is not as successful in B or R . The dependence of the models on Ω_0 can be gleaned from comparing the left and right panels of the various Figures. In general, for a fixed halo mass, lower values of Ω_0 will yield a larger disk mass and thus brighter luminosity. We have seen repeatedly that high values of Ω_0 invariably predict galaxies which are excessively faint as compared to observations.

In order to gain broader insight into the dependence of our results on the cosmological parameters, we generated data for the $\Omega_0 = 1$ case with $\Gamma = 0.2$ and $h = 0.45$ – 0.75 , and for $\Omega_0 = 0.2$ – 0.5 cases with $\Gamma = \Omega_0 h$ and $h = 0.55$ – 0.75 , both for the S distribution and for LC distributions with $f = 0.5$ and 0.75 . All were COBE normalized. Only a handful of these models produced values of $p > 0.001$ in any band, and those which did invariably had values of $\Omega_0 h \sim 0.2$, as required by current measurements. EdS models generally produce galaxies which are too faint, unless unacceptably low values of h are adopted, and produce too large a scatter, unless unacceptably low values of σ_8 are adopted. The best fitting models, both in terms of p and scatter, were LC distributions with COBE normalization, $\Omega_0 \sim 0.3$, and $h \sim 0.65$, similar to the best-fitting values obtained in earlier work (EL96; van den Bosch 2000) and in agreement with current estimates. As mentioned above, the S distribution predictions are generally too faint, due to the significant fraction of older galaxies arising from the high-redshift tail.

3.3 Spin-Parameter Distribution

We now turn to the issue of the spin-parameter distribution. Figures 9 and 10 correspond to the S and LC distributions from Figures 2 and 3, but with the joint probability distribution in λ and ν now taken into account. In the S distributions, this produces virtually no effect in K , as expected, but does broaden the distribution of points at each mass in the bluer bands. In every case, however, the TF scatter, is roughly similar to, or less than, that in Figure 2; the broadening has aligned along the TF relation itself. This arises from the fact that for a given mass, higher peaks (which collapse earlier and

have higher V_c) will have smaller spins leading to higher gas surface density and thus higher luminosities. A similar result is found in the LC case, though here the z_f distribution is weighted toward more recent epochs, exaggerating this effect and leading to a larger systematic reduction in the scatter, once our color selection criterion is enforced. Thus, in practice, accounting for the joint probability distribution in λ and ν can reduce the TF scatter by about 0.15 mag in B to 0.05 mag in K , for plausible cosmologies. Otherwise, the spin distribution does not have a great impact on the TF relation. As a corollary to this, we find that high-surface-brightness and low-surface-brightness disks, as distinguished by different λ or R_d in our model (see Figure 14), are predicted to lie on the same TF relation, as is in fact observed (Tully *et al.* 1998).

3.4 Chemical Evolution and the IMF

The role of chemical evolution is investigated in Figure 11 for the $\Omega_0 = 1$ S distribution and the Λ CDM LC distribution. Compared with their constant, solar-metallicity counterparts in Figures 2 and 3, these models have TF scatters which are systematically smaller by about 0.1 mag in all wavebands. This simply results from the fact that relative to constant metallicity systems, older disks (with higher V_c) will continually be forming populations of higher metallicity, and thus have a higher integrated luminosity. Conversely, younger systems will be relatively dimmer, so that models with an evolving metallicity content will naturally align more tightly along a luminosity-circular velocity relationship than those with constant Z .

In Figure 12 we examine the impact of changing the assumed IMF. The left panels depict a Salpeter IMF with $\alpha = 0.95$ (denoted as Salpeter-2), while the right panels represent a Scalo IMF (Scalo, 1986), each for the Λ CDM LC distribution. These IMFs both produce relatively more high-mass stars, thus yielding predictions which are excessively bright in the bluer bands. Note that the Salpeter-2 model matches reasonably in K , but not in any other band. This is yet another example of the importance of using multi-wavelength constraints to discriminate between models which may appear to fit in a single band.

4 A MODEL THAT WORKS

4.1 The TF Relation at $z=0$ and $z=1$

As an example of what can be accomplished with the theoretical framework presented here, we illustrate specifically the results for a COBE-normalized Λ CDM LC distribution with $f = 0.5$, $\Omega_0 = 0.3$, $h = 0.68$, a Salpeter IMF, and with the joint distribution in λ and ν , as well as chemical evolution. We refer to this particular model as the ‘A’ model. While this is not necessarily the best-fitting model over our entire parameter space, it does yield remarkable agreement with the data, as shown in Figure 13, and these model parameters fall nicely in line with current observational constraints. In addition to σ and p , the plots list the predicted normalizations and slopes [given by a and b in equation (1)]. The A model appears to fit the slope, normalization, and scatter of the TF relation reasonably well in all bands. The predicted scatter in B remains about 0.2 mag higher than observed, but there are several reasons one might expect this, given our model assumptions. In the next section, we show that features such as strong supernova feedback or a flatter density profile towards the core are not necessary to successfully predict many of the global spiral-galaxy properties

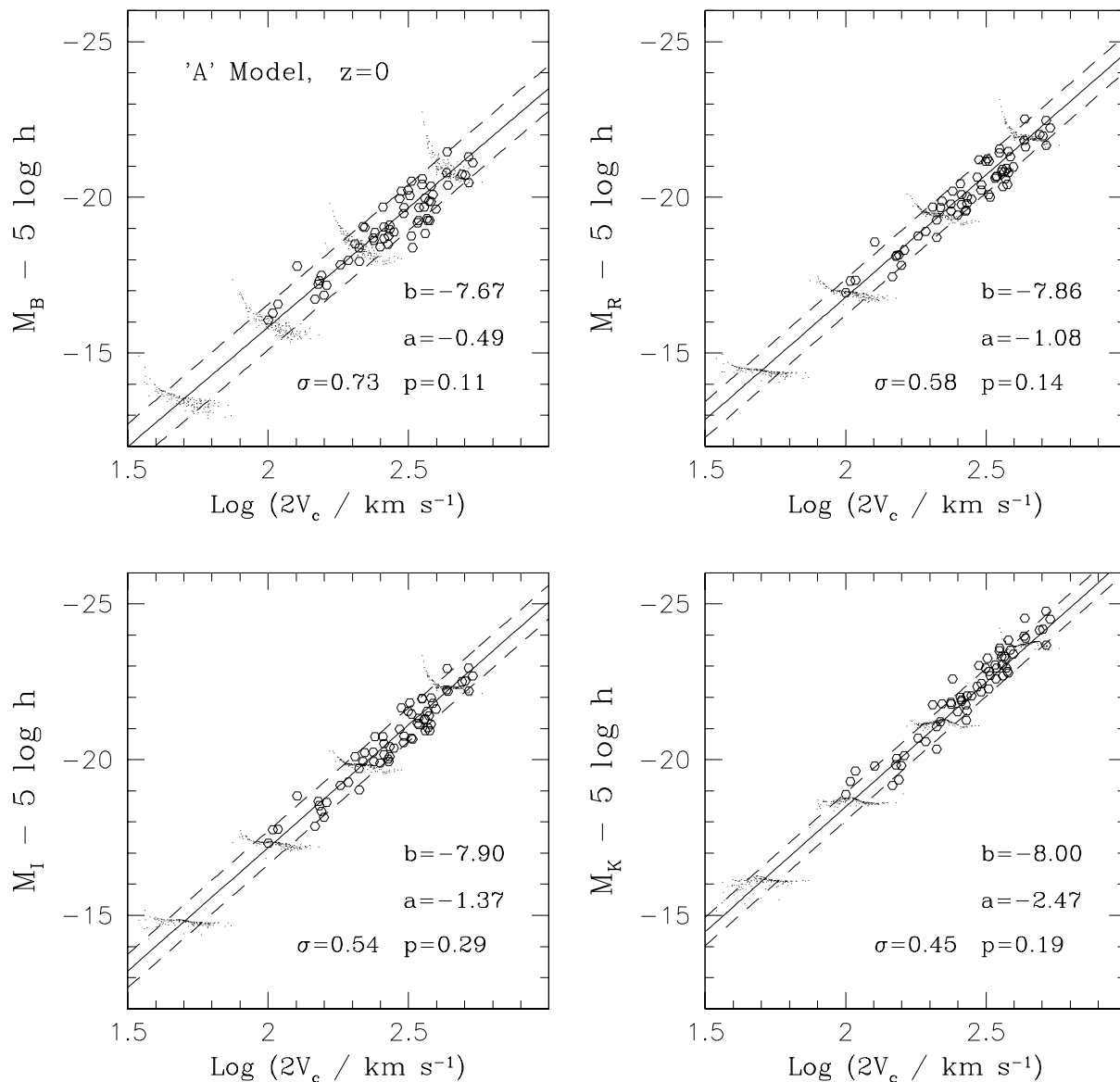


Figure 13. Agreement of the A model. Present-day TF predictions for the A model in B , R , I , and K for a COBE-normalized $f = 0.5$ LC distribution with $\Omega_0 = 0.3$, $h = 0.68$, a Salpeter IMF, including the joint distribution in λ and ν as well as chemical evolution. This model, denoted as the ‘A’ model, produces excellent agreement in all bands ($p > 0.10$) with roughly the correct amount of scatter ($\sigma \sim 0.4$ – 0.5).

investigated here. Thus, these features would tend only to produce small changes in the amount of gas available for star formation, so that their effects would be largely confined to B . Presumably, however, their inclusion would result in a slight dimming and tightening the B -band predictions, bringing them more in line with the observations.

Figure 14 shows the predictions of the A model for the TF relation at $z = 1$, together with 6 data points from Vogt *et al.* (1997) for spirals in the range $0.5 < z < 1.0$. These data have been corrected for dust. At $z = 1$ our model predicts larger values of a (i.e., lower zero-points) and steeper slopes for the TF relation in every band. This results in the TF relation becoming about 1 mag

brighter at 50 km s^{-1} , and about 2 mag brighter at 500 km s^{-1} in the B -band, but conspires to produce very little change at these scales in the K band. Moreover, the scatter in the TF relation in all bands at $z = 1$ is predicted to be roughly the same as that at $z = 0$, though we do not impose any color-selection criterion in the high-redshift case, since it is not as clear what the observational selections are. Though the B -band data shown are comprised of only 6 points, they have an intrinsic scatter consistent with that of the low- z data, and are fit by our model extremely well ($p = 0.32$), though, as in the $z = 0$ case, the predicted scatter is about 0.2 mag too large.

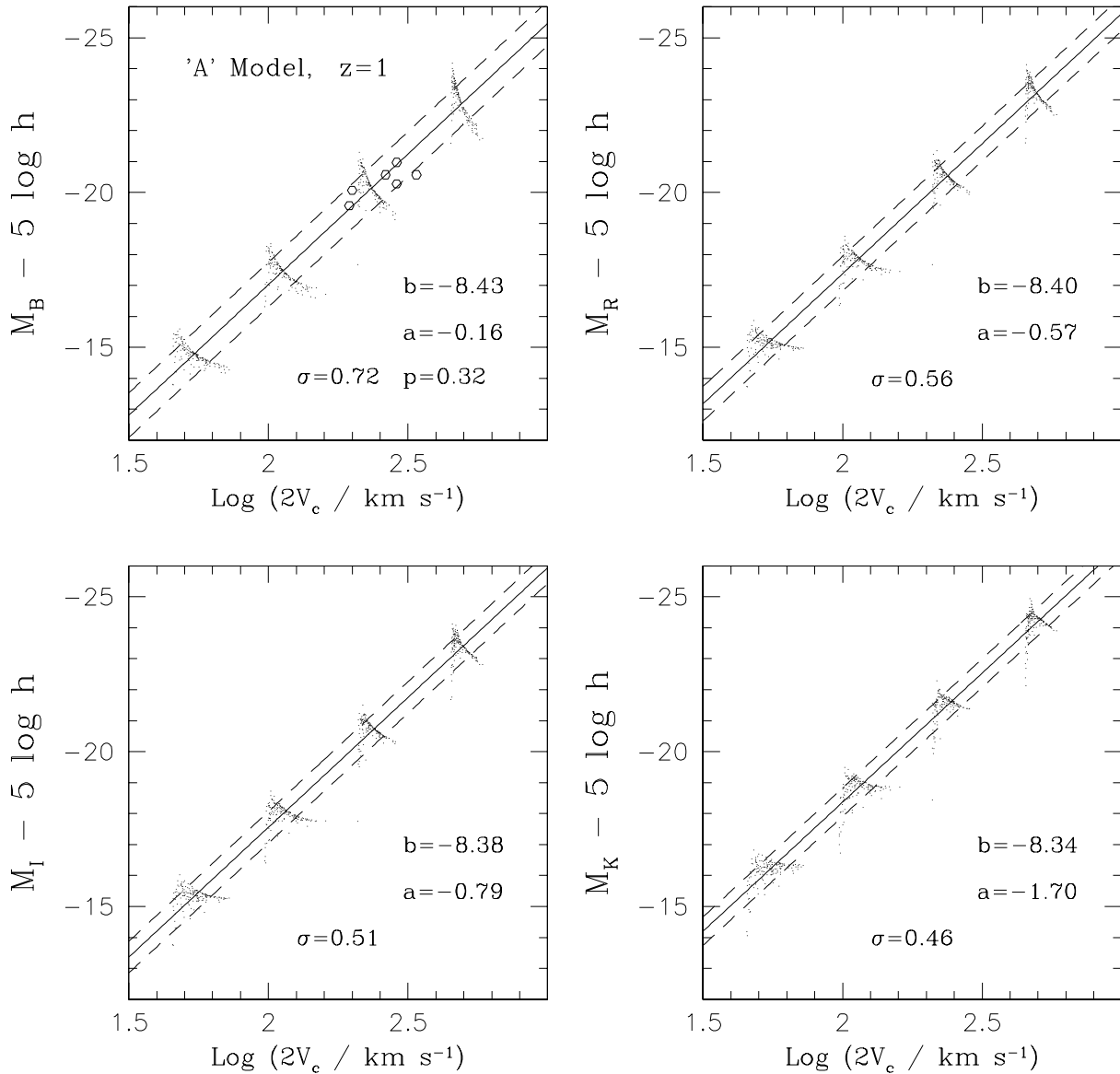


Figure 14. High-redshift predictions. TF prediction of the A model for $z = 1$, along with 6 B -band data point from Vogt *et al.* (1996) for spirals in the range $0.5 < z < 1$. The $z = 1$ prediction have steeper slopes (given by b) and lower zero-points (given by a), than the counterpart $z = 0$ predictions, resulting in a brighter B -band TF relation, but roughly a roughly similar relation in K .

4.2 The Luminosity Function and Surface-Brightness Distribution

The LF is given by $dn/dM_\lambda = (dn/dM)dM/dM_\lambda$ where dn/dM is the number density of objects, per unit mass, obtained from equation (4). An equation for dM/dM_λ is derived from the model outputs assuming the mass-magnitude relationship obeys a power law, which is an excellent assumption at these scales. For B -band magnitudes, we apply the dust correction formula of Wang & Heckman (1996) in calculating the LF.

The solid lines in Figure 15 are the predictions for the present-day B and K LFs for the A model. The horizontal error bars indicate the $1-\sigma$ error in our mass-magnitude power-law fits. No color

cuts have been imposed. The dashed line shows the B -band prediction without correcting for dust. The dot-dashed line is the B -band fit to the 2dF Survey data (Folkes *et al.* 1999), and the open squares are data from Zucca *et al.* (1997). The K -band data are taken from Gardner *et al.* (1997; open triangles) and Glazebrook *et al.* (1995; filled triangles).

The LF fits are where this model is weakest, as they rely heavily on the detailed number distribution of galaxies as predicted by the PS formalism, which is known to be inaccurate. We find that while the model reasonably approximates the faint end of the K -band data, it slightly underpredicts the number of galaxies around the knee (near $10^{12} M_\odot$) and overpredicts the bright end. We note

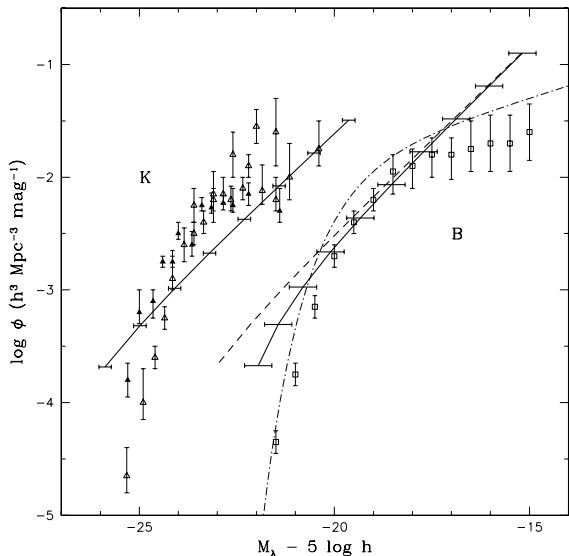


Figure 15. The luminosity function. B and K LF predictions of the A model (solid lines) together with $1\text{-}\sigma$ errors (horizontal error bars). The dashed line is the B -band prediction before correcting for dust. The dot-dashed line is the B -band fit to the 2dF Survey data (Folkes *et al.* 1999), and the open squares are data from Zucca *et al.* (1997). The K -band data are taken from Gardner *et al.* (1997; open triangles) and Glazebrook *et al.* (1995; filled triangles).

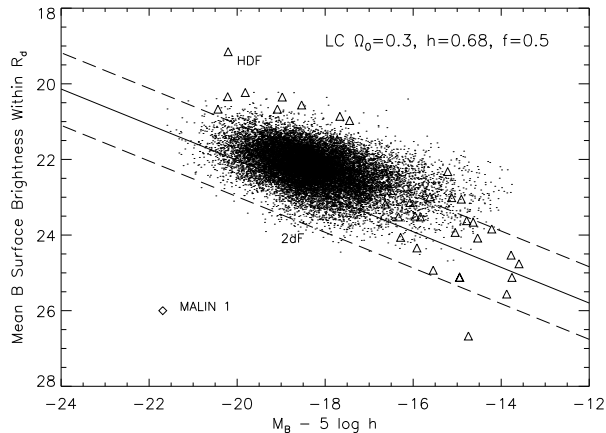


Figure 16. The surface-brightness–magnitude relation. A-model predictions for the mean B -band surface brightness as a function of magnitude (solid line) at $z = 0.4$, which corresponds to the mean redshift of the HDF data points (open triangles; taken from Driver *et al.* 1999). The dots are the data from Driver & Cross (2000), derived from the 2dF survey. The dashed lines show the $1\text{-}\sigma$ error in the prediction. We have also included the location of the anomalous LSB giant Malin 1.

that the bright end of the observed K -band LF is not presently well constrained, due to sample size and evolutionary effects. The dust-corrected B -band predictions yield reasonable agreement from the largest galaxies down to about $10^{11} M_{\odot}$, after which they overshoot the faint end by a considerable margin, as PS models are known to do. Given the shortcomings and limitations of the standard PS formalism, it is quite remarkable that the model yields as good agreement as it does over a factor of 100 in both number and luminosity.

Somerville & Primack (1999), using a modified PS prescription, do achieve slightly better agreement.

Generically, two explanations might resolve the discrepancy at the faint end in B , which is seen to persist even when more sophisticated formalisms than PS theory are implemented. One possibility is that our models overestimate the luminosity for a given mass. This would be the case, for example, if supernova feedback played a significant role in removing the gas. It is unclear to what extent the energy they release alters the global properties of spirals. If they serve only to “puff up” the gas distribution (Mac Low & Ferrara 1999), then our model would remain effectively unchanged. If they expel gas from the halo, this could alter our predictions. Inspection of Figure 15, however, reveals that, at low masses, feedback would have to reduce the predictions by many magnitudes in order to yield agreement. Somerville & Primack do find that the inclusion of feedback improves the agreement at the faint end in B , but still returns LF values on the high side. Our TF predictions, however, match B -band data down to $V_c = 50 \text{ km s}^{-1}$. Strong feedback would not only disrupt this agreement for low V_c , but also alter the predictions at other wavelengths. Some recent observations do indicate a break in the near-IR TF relation at $V_c \sim 90 \text{ km s}^{-1}$ (McGaugh *et al.* 2000), but these galaxies are found to be extremely gas rich, such that feedback is not sufficient to expel the gas. Fine tuning by supernovae of the gas mass available for star formation would be allowed by our model. This could improve both the TF predictions in B and slightly alleviate the LF discrepancy, but it appears unlikely that the latter problem can be solved entirely via feedback. We point out that the Schmidt law implicitly assumes supernova feedback which can redistribute gas within the disk and serves to delay star formation. It is only inflows and outflows which are not accounted for in our model, and detailed multi-phase ISM simulations seem to indicate that these are negligible and that spirals may be well-approximated as “island universes.” Note also that we may be implicitly assuming some influence of supernova (or other) feedback in keeping the specific angular momentum of the baryons equal to that of the halo.

Another possibility is that the model is simply predicting too many small halos. This may be due in part to the breakdown of the PS formalism in accurately describing the distribution of halos over these scales, but may also indicate that the assumed power spectrum itself is supplying too much power to these scales. Recent evidence suggests that current numerical models do indeed overpredict the number of dwarf halos surrounding a galaxy such as the Milky Way by an order of magnitude or more (Moore *et al.* 2000). Kamionkowski & Liddle (1999) show that this stark discrepancy can be addressed through plausible modifications to the power spectrum. This solution would reconcile the LF predictions with observations, while leaving the TF predictions untouched.

A very interesting test that is usually overlooked is that of the surface-brightness–magnitude relation. The solid line in Figure 16 shows our A-model prediction for the mean B -band surface brightness within the disk scale length, R_d [see equation (8)], as a function of magnitude; the dashed lines are the $1\text{-}\sigma$ bounds. The open triangles are data from Driver *et al.* (1999), who used a volume-limited sample derived from the Hubble Deep Field, and the dots are the data from Driver & Cross (2000) derived from the 2dF survey. We have also included the location of the anomalous LSB giant Malin 1. Although we are plotting model predictions for $z = 0.4$, the mean redshift for the galaxies in the HDF data set, the brightening of galaxies between $z = 0.1$ and 0.4 will have a minor impact on the outcome of the fit. No color cuts have been imposed. The first thing to note is that the data correspond to effective

surface brightness as defined in Driver *et al.* (1999), and therefore include a bulge component which is absent in our computed central surface brightness for an exponential disk^{**}. The first striking feature of the data itself is that there exists a correlation between absolute magnitude and surface brightness, as first discovered by Binggeli & Cameron (1991) for the Virgo population and later confirmed for the field population by Driver *et al.* (1999). Gratifyingly enough, our model predicts a similar correlation which produces a reasonable fit (albeit slightly fainter for the reasons detailed above and with a scatter only 15% larger than that *currently* observed). Until more complete surveys can determine the precise scatter of the surface-brightness–magnitude relation, it is too early to conclude if our model predicts a scatter that is in fact too large. As already proposed by Driver & Cross (2000), this relation offers a physical alternative to the “botanical” Hubble-galaxy classification scheme [see Fig. 4 in Driver & Cross (2000)], with the x-axis determined by the mass and the y-axis determined primarily by the angular momentum of the dark halo. Here we confirm that the x-axis is indeed determined by the mass, but the y-axis is determined both by the spin of the halo (λ) and by the redshift of formation (i.e., by the initial conditions). It is also reassuring to find that our model predicts that LSB giants like Malin-1 should be very rare objects (about $4\text{-}\sigma$ fluctuations), which agrees well with the observed paucity of these objects. As was the case for the TF predictions, most other models investigated (with different cosmogonies and so on) grossly failed to fit the data. Unlike the TF predictions, however, the surface-brightness predictions do depend sensitively on λ (which fixes the radial scale length), and thus provide a strong complementary constraint on the models.

5 CONCLUSIONS

We have constructed a largely analytic disk-galaxy model, built on that of HJ99, which incorporates such features as the halo formation-redshift distribution, the joint distribution in spin and peak height, the dependence on the cosmological model, and star formation with chemical evolution. Exploring the model’s predictions over a range of wavebands, we find that both parent-halo features and stellar evolution play a role in defining the TF relation and other disk-galaxy properties; the former fixes the overall relation and spread, while the latter fine tunes these to observed levels. Our investigation has yielded a number of specific results:

- We confirm that the spread in formation redshifts is the primary source of scatter in the TF relation. In agreement with previous studies, we predict a TF relation which generally broadens with decreasing V_c and exhibits increasingly large scatter towards bluer wavebands (HJ99; van den Bosch 2000; Somerville & Primack 1999).
- We find that $\Omega_0 = 1$ models are generally too faint to match the observed TF relation, but contrary to the claim of van den Bosch (2000), this result does not depend on the inclusion of adiabatic disk contraction, universal-halo profiles (Navarro, Frenk & White 1997), or the precise definition of V_c . We find that successful models tend to favor low values of $\Omega_0 h \sim 0.2$, and in particular $\Omega_0 \sim 0.3$ and $h \sim 0.65$ (assuming COBE normalization).^{††}

^{**} Note that the data points are slightly higher than the Freeman law (Freeman 1970; Driver *et al.* 1999).

^{††} Recent preliminary results from the BOOMERANG experiment (Lange *et al.* 2000) point to larger values of $\Omega_b h^2$. A higher baryon fraction would

- The inclusion of the spin-parameter distribution, with an anti-correlation with peak height, tends to act along the TF axis itself and can therefore slightly reduce the TF scatter in some models, but does not otherwise have a major impact on the TF relation. Thus, uncertainties in obtaining accurate λ distributions, such as nonlinear effects, proper calculation of binding energies, and so on, are likely unimportant. The spin distribution is important, however, in determining disk scale lengths and surface brightnesses, which can provide independent tests of the model.

- The incorporation of chemical evolution leads to older (younger) populations which are brighter (fainter), leading to a reduction of TF scatter of about 0.1 mag in all wavebands.

- Many models can be found to yield reasonable agreement with the data in one or two bands, but not in others. Typically, I and K data are the easiest to fit, since these wavelengths are largely detached from the star-formation history. Imposing multi-wavelength constraints, however, provides a strong discriminator among models.

- Models which yield the best agreement with TF data across *all* wavelengths have cosmological-parameter values in good agreement with current estimates, and require that most disks form in the range $0.5 < z < 2.0$, with little subsequent accretion, as suggested by Peebles (1999). In particular, the reasonable agreement in B seems to rule out very late collapse. The $f = 0.5$ LC distribution appears to represent a suitable choice for the range of halo formation redshifts. Note that this agreement is obtained with a spread in z_f of $\Delta z_f / (1 + z_f) \sim 0.5$, considerably larger than that suggested by the results of Eisenstein & Loeb (1996) and van den Bosch (2000), demonstrating the impact of regulating effects from stellar evolution and metal enrichment.

- Models fitting the TF relation at $z = 0$ also appear to obtain the correct, steeper B -band TF relation at $z = 1$, and predict a near-IR $z = 1$ TF relation which is essentially identical to the local one at the scales investigated.

- Successful models also roughly match the observed surface-brightness distribution of spirals and reasonably match the observed B - and K -band LFs.

- In general, this success argues that there is probably little room for stochasticity arising from other complicating effects, such as mergers. Spiral galaxies appear to behave like island universes (Mac Low & Ferrara 1999; Peebles 1999). Small variations to the disk baryon content from such mechanisms could still be tolerated, though their effects would be largely confined to the B band. Modeling these weaker effects might serve to improve the model’s prediction for the B -band TF relation and LF.

There are several features common to many SAMs which have not been incorporated into our framework, as these do not appear to strongly impact the properties investigated here. For example, we adopt an isothermal profile, rather than the universal form of Navarro, Frenk, & White (1997). While observations, as well as some simulations, indicate that real halos do resemble truncated isothermal spheres, rather than universal profiles (Sellwood 1999; Dubinski & Carlberg 1991; Spergel & Hernquist 1992), our model is clearly too steep in the core. For our purposes, however, changes to the profile of a halo with a fixed mass are only relevant inas-

brighten the TF predictions, but this could be counteracted by a slightly higher value of h (or by changing other input parameters so as to still remain within current constraints), so as to yield a similarly well-fitting model. Many of the conclusions presented here are robust with respect to the precise values of these various parameters.

much as they alter the local gas surface density and thus the SFR. This is similar to the effect of changing the spin parameter, and we have seen that our model changes relatively little over the broad range investigated in λ and thus Σ (HJ99). Jimenez *et al.* (1997) developed a similar disk-galaxy model, but explicitly incorporating the universal profile, and found little difference from the results of HJ99. The behavior of an isothermal profile at the core, however, will have the effect of making younger galaxies too bright in B . As discussed above, this might partially account for the slightly poorer TF fit and larger predicted scatter in B , as well as the discrepancy with the B -band LF.

While the assumption of monolithic disk collapse cannot be strictly accurate, accounting for adiabatic disk contraction also does not appear essential to predicting these disk properties. Moreover, adiabatic contraction tends to make spirals more dark-matter dominated at the core, whereas observations indicate that they are more baryon dominated (Sellwood 1999). Our model depends on an accurate assessment of V_c , and not on the details of disk formation, which do not affect our ultimate results. Similarly, the inclusion of a stability threshold criterion for star formation does not appear essential to our results, and some authors have argued against the importance of such a threshold (Ferguson *et al.* 1998).

Another key assumption in this model is that the specific angular momentum of the baryons is the same as that of the dark matter. This is a common assumption of analytic calculations (e.g. Fall & Efstathiou 1980; Mo, Mao & White 1998), but it has been argued from hydrodynamic simulations that this is not the case; cooling of gas leads to substructure which can couple with the halo, leading to loss of a sizeable fraction of the baryon angular momentum (e.g. Navarro & Benz 1991; Weil, Eke & Efstathiou; Navarro & Steinmetz 2000). The predictions of our model would thus be altered significantly, with much smaller disks, higher early star formation rates and different colors. Therefore we need to assume that such angular momentum loss does not occur in practice. It is fair to say that the question of how (or indeed if) baryon angular momentum is conserved is open at present, although there are plenty of ideas for how the coupling can be prevented. These include gas ejection from sub-units by supernovae (Efstathiou 2000), suppression of gas cooling until the halo is established with a smooth profile (Weil, Eke & Efstathiou 1998), prevention of formation of small halos by a cut-off in the power spectrum (Kamionkowski & Liddle 1999), or changing the nature of the dark matter (Spergel & Steinhardt 1999). In addition, van Kampen (2000) proposes that numerical simulations underestimate dynamical friction of the sub-units, leading to overestimated angular-momentum transfer.

A generic problem is the possibility that our model either over-predicts or under-predicts the amount of gas which is converted into disk stars, due to effects such as supernova feedback, the presence of hot x-ray gas, or enhanced star formation from late infall. Though we have assumed essentially featureless (in space and time) star formation, the addition or removal of large amounts of gas via such stochastic mechanisms would increase the scatter in the TF relation and shatter the agreement obtained here. To the extent that such processes result in smaller fluctuations to the amount of gas available for star formation, their effects would be confined primarily to B , where our models are indeed weakest. Mergers likely play only a very limited role. It is well known that classic spirals could not maintain their thin-disk structure in the case of extreme merging. EL96 found that excluding objects which had merged with a mass $> 20\%$ (as opposed to 50%) of the parent halo, only reduced the predicted I -band scatter by 20% , suggesting that accretion does not play a major role, or possibly induces

scatter along the near-infrared TF relation. Either way, this would imply that the TF relation at higher redshift looks similar to that at $z = 0$, and this is precisely what we find when comparing the $z = 0$ and $z = 1$ TF relations in I and K . Future work will be aimed at quantitatively assessing the precise impact of these various other mechanisms, as well as obtaining predictions for the high-redshift universe. While our model is a long way from providing a complete picture of galactosynthesis, our results suggest that future models addressing spiral properties must invariably incorporate detailed star formation, as well as initial conditions, and that features such as exponential disks, little or weak substructure, Schmidt-law star formation, and little gas inflow or outflow, should be generic predictions of more sophisticated modelling.

ACKNOWLEDGEMENTS

We wish to acknowledge the collaboration of A. F. Heavens, whose numerous contributions have greatly enhanced this work. We also wish to thank L. Wang for numerous helpful discussions and for providing numerical results pertinent to our cosmological models. This work was supported by grants NSF-AST-0096023, NSF-AST-9900866, NSF-AST-9618537, NASA NAG5-8506, DoE DE-FG03-92-ER40701 and by a PPARC Advanced Fellowship.

APPENDIX

The luminosity of an arbitrary stellar population can be computed analytically as follows. Simple stellar populations (SSPs) are the building blocks of any arbitrarily complicated population since the latter can be computed as a sum of SSPs, once the star-formation rate is provided. In other words, the luminosity of a stellar population of age t_0 (since the beginning of star formation), in waveband λ , can be written as:

$$L_\lambda(t_0) = \int_0^{t_0} \int_{Z_i}^{Z_f} L_{SSP,\lambda}(Z, t_0 - t) dZ dt \quad (11)$$

where the luminosity of the SSP is:

$$L_{SSP,\lambda}(Z, t_0 - t) = \int_{M_{min}}^{M_{max}} SFR(Z, M, t) l_\lambda(Z, M, t_0 - t) \frac{dN}{dM} dM \quad (12)$$

and $l_\lambda(Z, M, t_0 - t)$ is the luminosity of a star of mass M , metallicity Z , and age $t_0 - t$, Z_i and Z_f are the initial and final metallicities, dN/dM represents the IMF, M_{min} and M_{max} are the smallest and largest stellar mass in the population, and $SFR(Z, M, t)$ is the star formation rate at the time t when the SSP is formed.

The magnitudes for a SSP (normalized to $1 M_\odot$) as a function of age and metallicity, for a given photometric band UBVR_{IJK}, are approximated to within 4% by:

$$M_\lambda = -2.5 \times \sum_{i=0}^4 \sum_{j=0}^4 X^i C_\lambda(i+1, j+1) Y^j, \quad (13)$$

where

$$X = 5.76 + 3.18 \log \tau + 1.26 \log^2 \tau + 2.64 \log^3 \tau + 1.81 \log^4 \tau + 0.38 \log^5 \tau, \quad (14)$$

$$Y = 2.0 + 2.059 \log \zeta + 1.041 \log^2 \zeta + 0.172 \log^3 \zeta - 0.042 \log^4 \zeta, \quad (15)$$

and

$$\tau = \frac{t}{\text{Gyr}}, \quad \zeta = \frac{Z}{Z_{\odot}}. \quad (16)$$

Luminosities

are obtained simply from $L_{\lambda} = 10^{-0.4*(M_{\odot\lambda} - M_{\lambda})}$, where $M_{\odot\lambda} = \{5.61, 5.48, 4.83, 4.34, 4.13, 3.72, 3.36, 3.30, 3.28\}$ for $\{U, B, V, R, I, J, H, K, L\}$. The i and j values appear as exponents of X and Y , respectively, and as indices defining elements of the C_{λ} matrices, given by

$$C_U = \begin{pmatrix} -4.738 \times 10^{-1} & 4.029 \times 10^{-1} & -3.690 \times 10^{-1} & 1.175 \times 10^{-1} & -1.253 \times 10^{-2} \\ -2.096 \times 10^{-1} & -1.743 \times 10^{-1} & 1.268 \times 10^{-1} & -2.526 \times 10^{-2} & 8.922 \times 10^{-4} \\ -1.939 \times 10^{-2} & 1.401 \times 10^{-2} & -9.628 \times 10^{-3} & -1.754 \times 10^{-3} & 7.237 \times 10^{-4} \\ 2.671 \times 10^{-3} & -4.271 \times 10^{-4} & 2.470 \times 10^{-4} & 2.963 \times 10^{-4} & -7.334 \times 10^{-5} \\ -7.468 \times 10^{-5} & 6.676 \times 10^{-7} & 1.482 \times 10^{-6} & -9.594 \times 10^{-6} & 2.055 \times 10^{-6} \end{pmatrix}; (17)$$

$$C_B = \begin{pmatrix} -8.321 \times 10^{-1} & 5.972 \times 10^{-1} & -4.818 \times 10^{-1} & 1.356 \times 10^{-1} & -1.271 \times 10^{-2} \\ -1.223 \times 10^{-1} & -2.523 \times 10^{-1} & 2.117 \times 10^{-1} & -5.309 \times 10^{-2} & 3.716 \times 10^{-3} \\ -2.632 \times 10^{-2} & 2.468 \times 10^{-2} & -2.462 \times 10^{-2} & 4.163 \times 10^{-3} & 5.054 \times 10^{-5} \\ 2.835 \times 10^{-3} & -7.906 \times 10^{-4} & 9.653 \times 10^{-4} & -1.164 \times 10^{-5} & -3.800 \times 10^{-5} \\ -7.416 \times 10^{-5} & 1.120 \times 10^{-6} & -6.707 \times 10^{-6} & -5.615 \times 10^{-6} & 1.611 \times 10^{-6} \end{pmatrix}; (18)$$

$$C_V = \begin{pmatrix} -9.348 \times 10^{-1} & 7.376 \times 10^{-1} & -5.170 \times 10^{-1} & 1.182 \times 10^{-1} & -8.023 \times 10^{-3} \\ -9.521 \times 10^{-2} & -3.476 \times 10^{-1} & 2.379 \times 10^{-1} & -4.485 \times 10^{-2} & 1.303 \times 10^{-3} \\ -2.437 \times 10^{-2} & 4.413 \times 10^{-2} & -2.802 \times 10^{-2} & 2.202 \times 10^{-3} & 5.271 \times 10^{-4} \\ 2.625 \times 10^{-3} & -2.063 \times 10^{-3} & 9.257 \times 10^{-4} & 2.378 \times 10^{-4} & -8.471 \times 10^{-5} \\ -6.994 \times 10^{-5} & 2.842 \times 10^{-5} & 7.436 \times 10^{-7} & -1.424 \times 10^{-5} & 3.050 \times 10^{-6} \end{pmatrix}; (19)$$

$$C_R = \begin{pmatrix} -9.755 \times 10^{-1} & 8.121 \times 10^{-1} & -4.535 \times 10^{-1} & 5.553 \times 10^{-2} & 3.313 \times 10^{-3} \\ -7.346 \times 10^{-2} & -4.000 \times 10^{-1} & 1.983 \times 10^{-1} & -6.018 \times 10^{-3} & -5.621 \times 10^{-3} \\ -2.368 \times 10^{-2} & 5.415 \times 10^{-2} & -1.968 \times 10^{-2} & -5.209 \times 10^{-3} & 1.811 \times 10^{-3} \\ 2.502 \times 10^{-3} & -2.667 \times 10^{-3} & 1.376 \times 10^{-4} & 8.392 \times 10^{-4} & -1.845 \times 10^{-4} \\ -6.690 \times 10^{-5} & 4.003 \times 10^{-5} & 2.413 \times 10^{-5} & -3.043 \times 10^{-5} & 5.650 \times 10^{-6} \end{pmatrix}; (20)$$

$$C_I = \begin{pmatrix} -1.027 \times 10^0 & 8.951 \times 10^{-1} & -3.759 \times 10^{-1} & -1.908 \times 10^{-2} & 1.690 \times 10^{-2} \\ -4.672 \times 10^{-2} & -4.514 \times 10^{-1} & 1.411 \times 10^{-1} & 4.385 \times 10^{-2} & -1.440 \times 10^{-2} \\ -2.379 \times 10^{-2} & 6.399 \times 10^{-2} & -8.885 \times 10^{-3} & -1.425 \times 10^{-2} & 3.380 \times 10^{-3} \\ 2.414 \times 10^{-3} & -3.267 \times 10^{-3} & -7.741 \times 10^{-4} & 1.532 \times 10^{-3} & -3.012 \times 10^{-4} \\ -6.417 \times 10^{-5} & 5.166 \times 10^{-5} & 4.964 \times 10^{-5} & -4.843 \times 10^{-5} & 8.607 \times 10^{-6} \end{pmatrix}; (21)$$

$$C_J = \begin{pmatrix} -1.106 \times 10^0 & 1.043 \times 10^0 & -1.932 \times 10^{-1} & -1.715 \times 10^{-1} & 4.364 \times 10^{-2} \\ 1.122 \times 10^{-2} & -5.240 \times 10^{-1} & -6.001 \times 10^{-3} & 1.510 \times 10^{-1} & -3.228 \times 10^{-2} \\ -2.757 \times 10^{-2} & 7.613 \times 10^{-2} & 1.935 \times 10^{-2} & -3.358 \times 10^{-2} & 6.540 \times 10^{-3} \\ 2.502 \times 10^{-3} & -3.923 \times 10^{-3} & -2.956 \times 10^{-3} & 2.944 \times 10^{-3} & -5.274 \times 10^{-4} \\ -6.439 \times 10^{-5} & 6.234 \times 10^{-5} & 1.066 \times 10^{-4} & -8.371 \times 10^{-5} & 1.417 \times 10^{-5} \end{pmatrix}; (22)$$

$$C_K = \begin{pmatrix} -1.132 \times 10^0 & 1.296 \times 10^0 & -1.795 \times 10^{-1} & -2.391 \times 10^{-1} & 5.794 \times 10^{-2} \\ 6.838 \times 10^{-2} & -6.627 \times 10^{-1} & -5.987 \times 10^{-2} & 2.115 \times 10^{-1} & -4.319 \times 10^{-2} \\ -3.194 \times 10^{-2} & 1.009 \times 10^{-1} & 3.092 \times 10^{-2} & -4.459 \times 10^{-2} & 8.454 \times 10^{-3} \\ 2.649 \times 10^{-3} & -5.499 \times 10^{-3} & -3.923 \times 10^{-3} & 3.748 \times 10^{-3} & -6.625 \times 10^{-4} \\ -6.607 \times 10^{-5} & 9.556 \times 10^{-5} & 1.332 \times 10^{-4} & -1.038 \times 10^{-4} & 1.746 \times 10^{-5} \end{pmatrix}. (23)$$

REFERENCES

- Avila-Reese, V., Firmani, C., & Hernandez, X. 1998, *ApJ*, 505, 37
- Bardeen, J. M. *et al.* 1986, *ApJ*, 304, 15
- Binggeli, B. & Cameron, L. M. 1991, *A&A*, 252, 27
- Bullock, J. S. *et al.* 1999, *ApJ*, 458, 419
- Bunn, E. F. & White, M. 1997, *ApJ*, 480, 6
- Catelan, P. & Theuns, T. 1996, *MNRAS*, 282, 436
- Dalcanton, J. J., Spergel, D. N., & Summers, F. J. 1997, *ApJ*, 482, 659
- Driver, S. P. *et al.* 1999, *ApJL*, 526, 69
- Driver, S. P. & Cross N. 2000, astro-ph/0004201
- Dubinski, J. & Carlberg, R. G. 1991, *ApJ*, 378, 496
- Efstathiou, G. 2000, *MNRAS*, submitted (astro-ph/0002245)
- Eisenstein, D. J. & Loeb, A. 1996, *ApJ*, 459, 432 (EL96)
- Fall, S. M. & Efstathiou, G. 1980, *MNRAS*, 193, 189
- Firmani, C. & Avila-Reese, V. 1998, *ASP Conf. Ser.*, 176, 406
- Ferguson, A. M. N. *et al.* 1998, *ApJL*, 506, 19
- Folkes, S. R. *et al.* 1999, *MNRAS*, accepted (astro-ph/9903456)
- Freeman, K. C. 1970, *ApJ*, 160, 811
- Gardner, J. P. *et al.* 1999, *ApJ*, 480, 99
- Glazebrook, K. *et al.* 1995, *MNRAS*, 275, 169
- Heavens, A. F. & Jimenez, R. 1999, *MNRAS*, 305, 770 (HJ99)
- Heavens, A. F. & Peacock, J. 1988, *MNRAS*, 232, 339
- Jimenez, R. *et al.* 1997, *MNRAS*, 292, L5
- Jimenez, R. *et al.* 1998, *MNRAS*, 299, 123
- Jimenez, R. *et al.* 2000, *MNRAS*, *ApJ*, 532, 152
- Kamionkowski, M. & Buchalter, A. 2000, *PRL*, submitted (astro-ph/0001045)
- Kamionkowski, M. & Liddle, A. R. 1999, astro-ph/9911103
- Kennicutt, R. 1998, *ApJ*, 498, 5541
- Lacey, C. & Cole, S. 1993, *MNRAS*, 262, 627
- Lacey, C. & Cole, S. 1994, *MNRAS*, 271, 676
- Lange, A. E. *et al.* 2000, astro-ph/0005004
- Lemson, G. & Kauffmann, G. 1999, *MNRAS*, 302, 111
- Mac Low, M.-M. & Ferrara, A. 1999, *ApJ*, 513, 142
- McGaugh, S. S. *et al.* 2000, astro-ph/0003001
- Mo, H. J., Mao, S., & White, S. D. M. 1998, *MNRAS*, 295, 319
- Mo, H. J. & Mao, S. 2000, astro-ph/0002451
- Moore, B. *et al.* 2000, astro-ph/0002308
- Navarro, J. F. & Benz, W. 1991, *ApJ*, 380, 320
- Navarro, J. F., Frenk, C. S., & White, S. D. M. 1997, *ApJ*, 490, 493
- Navarro, J. F. & Steinmetz, M. 2000, *ApJ*, submitted (astro-ph/0001003)
- Pagel, B. E. J. 1997, *Nucleosynthesis and Chemical Evolution of Galaxies* (Cambridge: Cambridge University Press)
- Peacock, J. A. & Dodds, S. J. 1994, *MNRAS*, 267, 1020
- Peebles, P. J. E. 1999, astro-ph/9910234
- Percival, W. J., Miller, L., & Peacock, J. A. 2000, astro-ph/0002328
- Pettini, M. *et al.* 1999, *ApJ*, 510, 576
- Sasaki, S. 1994, *PASJ*, 46, 427
- Scalo, J. 1986, *Fundam. Cosmic Phys.*, 11, 1
- Sellwood, J. A. 1999, astro-ph/9903184
- Silk, J. 1997, *ApJ*, 481, 703
- Somerville, R. S. & Primack, J. R. 1999, *MNRAS*, 310, 1087
- Spergel, D. N. & Hernquist, L. 1992, *ApJL*, 397, 75
- Spergel, D. N. & Steinhardt, P. J. 1999, *PRL*, 84, 3760
- Tully, R. B. *et al.* 1998, *AJ*, 115, 2264
- Tytler, D. *et al.* 1999, *ApJ*, *AJ*, 117, 63
- Ueda, H. *et al.* 1994, *PASJ*, 46, 319
- van den Bosch, F. C. 2000, *ApJ*, 530, 177
- van Kampen, E. 2000, in preparation
- Viana, P. T. P. & Liddle, A. R. 1996, *MNRAS*, 281, 323
- Vogt, N. P. *et al.* 1997, *ApJL*, 479, 121
- Weil, M. L., Eke, V. R., & Efstathiou, G. 1998, *MNRAS*, 300, 773
- Willick, J. A. *et al.* 1995, *ApJ*, 446, 12
- Willick, J. A. *et al.* 1996, *ApJ*, 457, 460
- Willick, J. A. *et al.* 1997, *ApJS*, 109, 333
- Wang, B. & Heckman, T. 1996, *ApJ*, 457, 645
- Wang, L. 1999, private communication
- Wang, L. & Steinhardt, P. J. 1998, *ApJ*, 508, 483
- Zucca, E. *et al.* 1997, *A&A*, 326, 477